

# Institutionen för systemteknik

## Department of Electrical Engineering

**Examensarbete**

# **Development and Analysis of Synchronization Process Control Algorithms in a Dual Clutch Transmission**

Examensarbete utfört i Fordonssystem  
vid Tekniska högskolan i Linköping  
av

**Andreas Gustavsson**

LITH-ISY-EX--09/4191--SE

Linköping 2009



**Linköpings universitet**  
**TEKNISKA HÖGSKOLAN**



# Development and Analysis of Synchronization Process Control Algorithms in a Dual Clutch Transmission

Examensarbete utfört i Fordonssystem  
vid Tekniska högskolan i Linköping  
av

**Andreas Gustavsson**

LITH-ISY-EX--09/4191--SE

Handledare: **Christofer Sundström**  
ISY, Linköpings universitet  
**Tobias Berndtson**  
GM Powertrain Sweden

Examinator: **Lars Eriksson**  
ISY, Linköpings universitet

Linköping, 23 February, 2009



	<b>Avdelning, Institution</b> Division, Department  Division of Vehicular Systems Department of Electrical Engineering Linköpings universitet SE-581 83 Linköping, Sweden	<b>Datum</b> Date  2009-002-23
	<b>Språk</b> Language  <input type="checkbox"/> Svenska/Swedish <input checked="" type="checkbox"/> Engelska/English  <input type="checkbox"/> _____	<b>Rapporttyp</b> Report category  <input type="checkbox"/> Licentiatavhandling <input checked="" type="checkbox"/> Examensarbete <input type="checkbox"/> C-uppsats <input type="checkbox"/> D-uppsats <input type="checkbox"/> Övrig rapport <input type="checkbox"/> _____
<b>URL för elektronisk version</b> <a href="http://www.fs.isy.liu.se">http://www.fs.isy.liu.se</a>		
<b>Titel</b> Title Development and Analysis of Synchronization Process Control Algorithms in a Dual Clutch Transmission  <b>Författare</b> Andreas Gustavsson Author		
<b>Sammanfattning</b> Abstract  <p>The Dual Clutch Transmission (DCT) is a relatively new kind of transmission which shows increased efficiency and comfort compared to manual transmissions. Its construction is much like two parallel manual transmissions, where the gear-shifts are controlled automatically. The gear-shift of a manual transmission involves a synchronization process, which synchronizes and locks the input shaft to the output shaft via the desired gear ratio. This process, which means transportation of a synchronizer sleeve, is performed by moving the gear shift lever which is connected to the sleeve. In a DCT, there is no mechanical connection between the gear-shift lever and the sleeve. Hence, an actuator system, controlled by a control system, must be used.</p> <p>This report includes modelling, control system design and simulation results of a DCT synchronization process. The thesis work is performed at GM Powertrain (GMPT) in Trollhättan. At the time of this thesis, there is no DCT produced by GM, and therefore the results and conclusions rely on simulations. Most of the used system parameters are reasonable values collected from employees at GMPT and manual transmission literature.</p> <p>The focus of the control design is to achieve a smooth, rather than fast, movement of the synchronizer sleeve. Simulations show that a synchronization process can be performed in less than 400 ms under normal conditions. The biggest problems controlling the sleeve position occur if there is a large amount of drag torque affecting the input shaft. Delay problems also worsen the performance a lot. An attempt to predict the synchronizer sleeve position is made and simulations shows advantages of that.</p> <p>Some further work is needed before the developed control software can be used on a real DCT. Investigations of sensor noise robustness and the impact of dogging forces are the most important issues to be further investigated. Implementation of additional functionality for handling special conditions are also needed.</p>		
<b>Nyckelord</b> Keywords dct, dsg, amt, synch, synchronizer, detent, dogging, gear shift, synchronization		



# Abstract

The Dual Clutch Transmission (DCT) is a relatively new kind of transmission which shows increased efficiency and comfort compared to manual transmissions. Its construction is much like two parallel manual transmissions, where the gear-shifts are controlled automatically. The gear-shift of a manual transmission involves a synchronization process, which synchronizes and locks the input shaft to the output shaft via the desired gear ratio. This process, which means transportation of a synchronizer sleeve, is performed by moving the gear shift lever which is connected to the sleeve. In a DCT, there is no mechanical connection between the gear-shift lever and the sleeve. Hence, an actuator system, controlled by a control system, must be used.

This report includes modelling, control system design and simulation results of a DCT synchronization process. The thesis work is performed at GM Powertrain (GMPT) in Trollhättan. At the time of this thesis, there is no DCT produced by GM, and therefore the results and conclusions rely on simulations. Most of the used system parameters are reasonable values collected from employees at GMPT and manual transmission literature.

The focus of the control design is to achieve a smooth, rather than fast, movement of the synchronizer sleeve. Simulations show that a synchronization process can be performed in less than 400 ms under normal conditions. The biggest problems controlling the sleeve position occur if there is a large amount of drag torque affecting the input shaft. Delay problems also worsen the performance a lot. An attempt to predict the synchronizer sleeve position is made and simulations shows advantages of that.

Some further work is needed before the developed control software can be used on a real DCT. Investigations of sensor noise robustness and the impact of dogging forces are the most important issues to be further investigated. Implementation of additional functionality for handling special conditions are also needed.



# Acknowledgments

This project has been carried out at GM Powertrain in Trollhättan and I would like to thank everyone there for their support and friendliness. Special gratitude goes to Tobias Berndtson, Mikael Johansson and Ludvig Franzén.

Additionally, I would like to thank my university examiner Lars Eriksson and supervisor Christofer Sundström at the division of Vehicular Systems, Linköping University.

Finally I give a special acknowledgement to Madeleine, Bamse and the rest of my family for being there when I was not.

*Thank you!*



# Contents

<b>1</b>	<b>Introduction</b>	<b>1</b>
1.1	Background and Objectives . . . . .	1
1.2	Limitations and Assumptions . . . . .	4
1.3	Method . . . . .	4
1.4	Outline . . . . .	5
1.5	Notation . . . . .	5
<b>2</b>	<b>System Description and Modeling</b>	<b>7</b>
2.1	Actuator System . . . . .	10
2.1.1	Hydraulic System . . . . .	11
2.1.2	Actuator Fork . . . . .	12
2.2	Synchronizer . . . . .	14
2.2.1	The Synchronizer Sleeve . . . . .	18
2.2.2	The Synchronizer Friction Rings . . . . .	22
2.3	The Input and Output Shafts . . . . .	24
<b>3</b>	<b>System Transfer Function</b>	<b>27</b>
<b>4</b>	<b>Controller Implementation</b>	<b>29</b>
4.1	State Machine . . . . .	32
4.2	Observer . . . . .	35
4.2.1	Fork Velocity and Position Prediction . . . . .	36
4.2.2	Detent and Static/Coulomb Friction Estimation . . . . .	37
4.2.3	Input Shaft Drag Estimation . . . . .	37
4.3	Controller . . . . .	40
4.3.1	Transportation . . . . .	41
4.3.2	Synchronization . . . . .	46
4.4	Pressure Calculation . . . . .	52
<b>5</b>	<b>Results</b>	<b>55</b>
5.1	Normal Conditions . . . . .	57
5.2	Cold Conditions . . . . .	61
5.3	Different Sample Times . . . . .	64
5.4	Different Detent Compensations . . . . .	65
5.5	Parameter Variations and Sensor Backlash . . . . .	67

---

5.6 Fork Position Prediction . . . . .	70
<b>6 Discussion</b>	<b>73</b>
<b>7 Future Work</b>	<b>75</b>
<b>8 Variable and Parameter Lists</b>	<b>77</b>
<b>Bibliography</b>	<b>81</b>
<b>A Transfer Function Calculation</b>	<b>83</b>
A.1 Equation 3.2 . . . . .	83
A.2 Equation 3.3 . . . . .	83
A.3 Equation 3.4 . . . . .	84
A.4 Equation 3.5 and 3.6 . . . . .	84
<b>B Synchronization Force Calculation</b>	<b>85</b>
<b>C State Machine Functionality</b>	<b>91</b>

# Chapter 1

## Introduction

Awareness of the environmental effects of emissions has a big impact on the powertrain development in the automotive industry. Together with comfort demands it has led to the development of Dual-Clutch Transmissions (DCT), also called Direct-Shift Gearbox (DSG) or Twin-Clutch Gearbox. A DCT is similar to a regular manual transmission, but consists of two input shafts, clutches and output shafts instead of one. Figure 1.1 shows a schematic view of a DCT. The odd gears are placed at one of the input and output shafts, and the even gears at the other pair. The advantage of using this configuration is that the next gear supposed to be used, is prepared before the shift occurs, which is called preselection. When changing gear, one clutch is disengaged at the same time as the other one is engaged. This results in a smooth gear shift with high efficiency and at the same time a good shift comfort. For further general information about Dual-Clutch Transmissions, readers are recommended [2] and [5].

### 1.1 Background and Objectives

The task of the clutch in a manual transmission is to disengage the gear box input shaft from the engine, which is needed when changing gear ratio. An example of a gearbox with two gears is shown in figure 1.2, where the dark parts rotates free from the bright parts.  $g_p$  represent one gear with gear ratio  $i_p$  and  $g_n$  another with ratio  $i_n$ . To drive the transmission at a specific gear ratio, the input shaft must be connected to the output shaft through the gear wheels of the actual gear. This is performed by moving the sleeve in the figure against the actual gear wheel. Splines in the sleeve will mesh with splines at the gear wheel so they are locked with each other. To enable this mesh, the input and output shaft angular velocities must be synchronized ( $\omega_i = -i\omega_o$ ). The mechanism between the gears, which enables this synchronization and gear ratio locking, is called synchronizer. The space at the input shaft where the synchronizer is placed is called the gear gate and thus handles one gear in positive direction ( $g_p$ ) and one in negative direction ( $g_n$ ).

The movement of the synchronizer sleeve is controlled by the gear shift lever in a manual transmission. In a DCT, there is no mechanical connection between

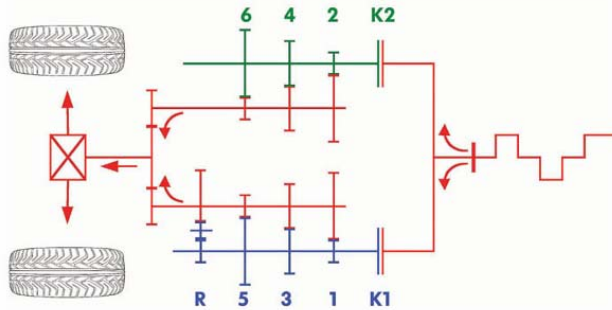


**Figure 1.1.** This figure shows a schematic view of a Dual-Clutch Transmission.  $K1$  and  $K2$  are the clutches of the odd and even input shaft respectively. Note that the odd gears and the reverse is placed at the odd input shaft and vice versa. In reality, one of the input shafts is nestled inside the other. One of the clutches is always disengaged which result in that the next gear can be prepared before the shift takes place.

the gear shift lever and the synchronizer. Instead, the synchronizer is controlled by an actuator system.

The thesis work is performed at GM Powertrain (GMPT) in Trollhättan, Sweden. The objective is to develop and analyze a control strategy of the synchronization process (also called fork control). Additional objectives are to identify how different parameters affects the performance of the synchronization process. This will also include analysis of the impact of delays, sampling times and sensor resolutions.

Demands on the synchronization process are that it should be performed fast (a few tenth of a second) and with little noise, which are two conflicting criterions.

The actuators of a synchronizer system can either be electro mechanical or hydraulic mechanical. At the time of this thesis, a hydraulic system with pressure valves is most common on the market and therefore treated in this investigation.

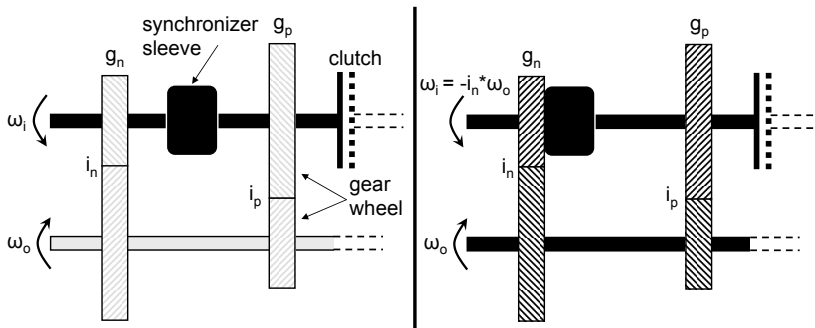


**Figure 1.2.** An example of a transmission with two gears. Dark parts rotates free from bright parts. The sleeve is placed between the two gears  $g_p$  and  $g_n$  and in the right picture the sleeve has locked the input shaft to the gear wheel of  $g_n$  and consequently the input shaft to the output shaft.

## 1.2 Limitations and Assumptions

Since there is no DCT produced by GMPT at the time of this thesis, information required for the modeling process and parametrisation are collected from employees at the company and manual transmission documentations. For some parameters it is hard to get reasonable values, and other studies where different values are used for such parameters may show different results.

The verification process is restricted to rely on a simulation model. This means that for example the demand of little noise during gearshifts is impossible to verify. This will be restricted to the analysis of which speed the synchronizer sleeve comes in contact with other parts.

Another limitation is that there is little information about similar work to be found, simply because this is a relatively new technique.

The work is restricted to only include engagement, and not disengagement, of the synchronizer sleeve. Neither are any strategies of which vehicle speed a gear shift should be performed, nor any preselection strategies treated here.

In the reality, synchronizers are placed at the input shaft for some gears and at the output shaft for others. But only synchronizers placed at the input shaft are treated here. Nevertheless, there is only a slight difference between the two cases regarding how to model the synchronization torque.

## 1.3 Method

Initially, a study about DCT and synchronizers is performed. This include discussions and meetings with different employees at the company and a literature study, which leads to a mathematical model of the synchronization process. The development and analysis parts of the work are made in Matlab Simulink and the developed control strategies is implemented as a Simulink block. An existing Simulink model of the physical system is available at GMPT and it is used for simulation and verification of the control strategies. It is from here on referred to as the simulation plant. Some small modifications of the simulation plant has been made.

Parallel to the development work, a study of modeling and control literature is performed.

## 1.4 Outline

- Chapter 2** This chapter contains a detailed system description. The system is divided in several subsystems and for each one some equations are presented.
- Chapter 3** A transfer function based on the equations in chapter 2 is developed and presented.
- Chapter 4** This chapter presents the developed and implemented control system. It is divided into four subsystems/Simulink blocks, of which the input and output signals are listed and the main functionality described.
- Chapter 5** The simulation results are presented and analyzed in this chapter.
- Chapter 6** A final discussion about results.
- Chapter 7** A final discussion about future works.
- Chapter 8** Lists of most of the used variables and parameters are placed here.

## 1.5 Notation

This report include some mathematics and the notation is explained here.

$\dot{l}(t)$  Time derivative of  $l(t)$ .

$\mathbf{L}(s), \mathbf{F}(s)$  Laplace transforms of  $l(t)$  and  $F(t)$ . Note that forces are represented by capital letters in the time domain while other variables are represented by lower case letters .

$l(k)$  Discrete representation of the continuous variable  $l(kT_s)$ ,  $k = 0, 1, 2, \dots$  where  $T_s$  is the sample time.

$\mathbf{L}(z)$  Z-transform of  $l(k)$ .



## Chapter 2

# System Description and Modeling

The system which is involved in the synchronization process can basically be divided into four main parts; the actuator system, the synchronizer mechanism, the input and output shafts and the control software. Figure 2.1 shows a general view of the system and the available sensor signals  $y_1$ ,  $y_2$  and  $y_3$ . In this thesis, the actuator system includes a hydraulic system, a fork and a piston connected to the hydraulic system in one end and to the fork at the other end. The synchronizer consists of a sleeve, a hub and friction rings placed between the sleeve and the gear wheels. The object is to move the sleeve so it locks with the gear wheel of the requested gear. This is performed by forces acting on the different sides of the piston end due to different pressures in the hydraulic system. Figure 2.2 shows a general view of the signal flow in the system. When the synchronizer sleeve is in contact with the friction rings, the applied actuator force generates a torque which accelerates or decelerates the input shaft angular velocity towards the angular velocity of the gear wheel. After this, the movement of the sleeve can continue towards the gear wheel.

Some of the system parameter values are truly uncertain. These are mentioned as uncertain and a more accurate calibration of them is needed. It is important to try some different values of these uncertain parameters, and also to try different values of them compared to what are being used in the simulation plant.

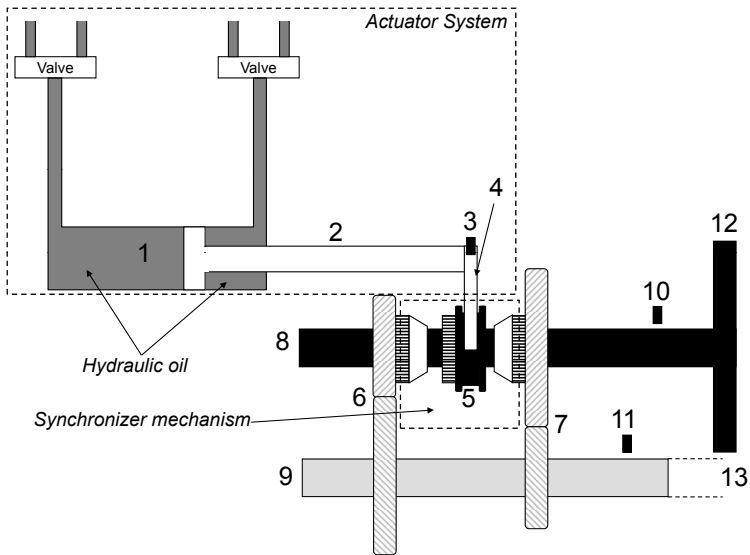


**Figure 2.1.** System overview. The different parts are: 1) Hydraulic system, 2) Actuator piston, 3) Actuator fork position sensor ( $y_1$ ), 4) Actuator fork, 5) Synchronizer sleeve and hub, 6) Lower gear, 7) Higher gear, 8) Input shaft, 9) Output shaft, 10) Input shaft angular velocity sensor ( $y_2$ ), 11) Output shaft angular velocity sensor ( $y_3$ ), 12) Clutch (connection to engine), 13) Connection to wheels

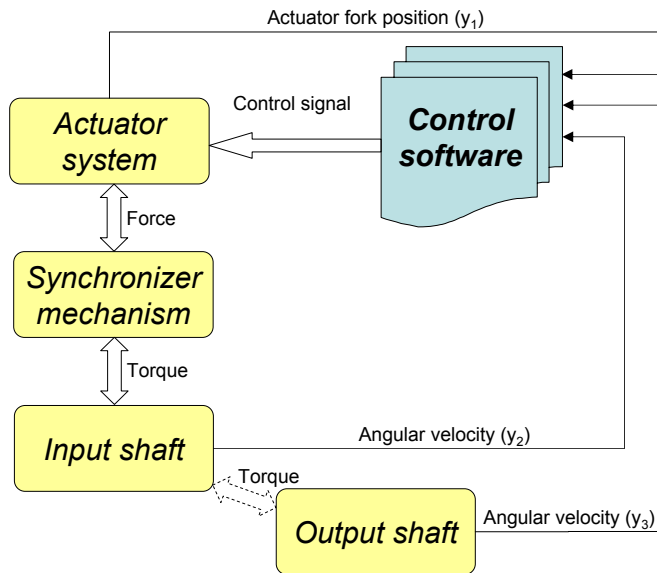


**Figure 2.2.** A flowchart of the synchronization process involved subsystems. An electric current from the control software controls the actuator system pressure valves. In this thesis, the control signals are assumed to be requested pressure. The actuator system force acts on the synchronizer mechanism and at a specific position, this force propagates on the friction rings and generate a torque on the input shaft. The fork position, the input shaft angular velocity and the output shaft angular velocity are the available measurements.

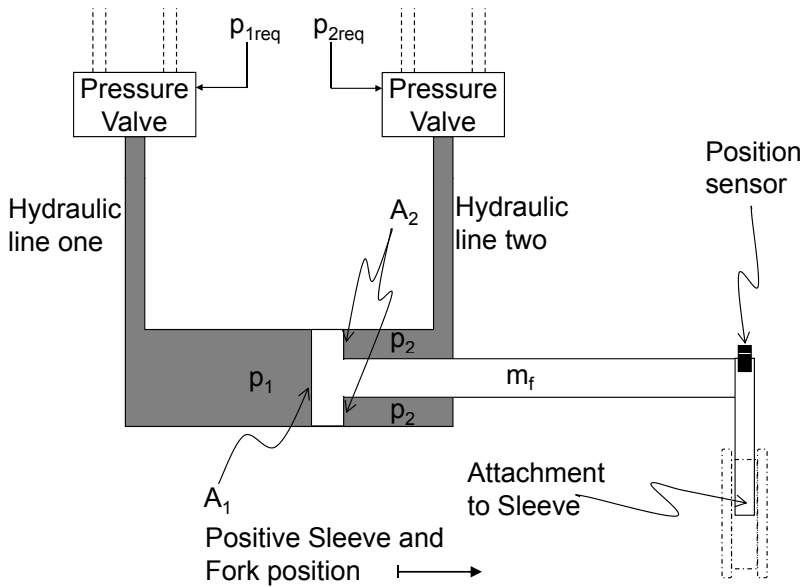


**Figure 2.3.** A schematic view of the actuator system. Note that  $A_2$  is the total area in contact with the hydraulic oil at the second side and that it is smaller than  $A_1$ .

## 2.1 Actuator System

Figure 2.3 shows a schematic view of the actuator system of this thesis. It consists of two hydraulic lines, each connected to the piston, but at different sides. When the lines are pressurized, a difference in force at the two sides will cause the piston and the fork to accelerate. The end of the fork is attached to the synchronizer sleeve and the position sensor is attached at the end of the piston.

### 2.1.1 Hydraulic System

The hydraulic pressures depends on the valve position, which for such valves depends on an electric current. The relationship is nonlinear and the electric current corresponding to a specific pressure request needs to be taken from a calibrated look-up table. However, this is not considered in this thesis since the control signal is requested pressure. Although, some parameters are used to model the delay and dynamics of the valve. These values are taken from [10] and are used to create a three parameter process model [3] with a static gain of one.

$$\begin{aligned} a_h \dot{p}_1(t) + p_1(t) &= p_{1req}(t - T_{ad}) \\ a_h \dot{p}_2(t) + p_2(t) &= p_{2req}(t - T_{ad}) \end{aligned} \quad (2.1)$$

$p_i$  is the pressure in line  $i$  and  $p_{ireq}$  is the corresponding control signal (requested pressure).  $T_{ad}$  is the actuator delay and  $a_h$  is the time constant for the dynamics.

The force  $F_{a,press}$  acting on the piston end should then be

$$F_{a,press}(t) = A_1 p_1(t) - A_2 p_2(t) \quad (2.2)$$

Index  $a$  is used in some variables and parameters which shows that they are related to the actuator system. There is also a maximum pressure of  $p_{max}$  in the two hydraulic lines.

### 2.1.2 Actuator Fork

The actuator piston and fork can be treated as one object which is attached to the hydraulic system at one side and to the synchronizer sleeve at the other side. It is most probable that some friction forces affects the piston and fork, and according to [10] there are viscous friction related to the hydraulic flow with magnitude of  $\mu_{a,vf}$ , which can be treated as a friction force acting on the piston. There may also be some static and coulomb friction which are denoted as  $f_{a,static}$  and  $f_{a,coulomb}$  respectively. The values of the friction parameters are truly uncertain according to [10], but their internal relationship should be  $f_{a,coulomb} < f_{a,static} \ll \mu_{a,vf}$ . The static and coulomb friction can be described as

$$F_{a,sc}(t) = \begin{cases} -\text{sign}(F_{a,r}(t)) \min(f_{a,static}, |F_{a,r}(t)|) & \text{if } \dot{l}_f(t) = 0 \\ -\text{sign}(\dot{l}_f(t)) f_{a,coulomb} & \text{else} \end{cases} \quad (2.3)$$

where  $l_f$  is the fork position,  $F_{a,r}$  is the sum of all other forces acting on the actuator piston and fork and index *sc* means "static coulomb". The viscous friction effects are modeled as

$$F_{a,vf}(t) = -\mu_{a,vf} \dot{l}_f(t) \quad (2.4)$$

According to [6], there is a dislocation of  $x_{fork}$  between the sensor position and the sleeve attachment when a force  $f_{app}$  is applied at the piston and the mechanism is in equilibrium (see figure 2.4). This displacement is modeled as a spring and a damper between the fork and the sleeve. The spring rate  $k_{fs}$  is calculated as  $k_{fs} x_{fork} = f_{app} \Leftrightarrow k_{fs} = \frac{f_{app}}{x_{fork}}$  and the damping rate is approximated as  $c_{fs} = k_{fs} \cdot 10^{-3}$ . The force between the fork and the sleeve should then be

$$F_{fs}(t) = k_{fs}(l_f(t) - l_s(t)) + c_{fs}(\dot{l}_f(t) - \dot{l}_s(t)) \quad (2.5)$$

where  $l_s$  is the synchronizer sleeve position and index *fs* means "fork sleeve".

If it is assumed that the whole mass of the actuator piston and fork  $m_f$ , is located at the hydraulic system side of the spring and damper effects, the equation of motion follow as

$$m_f \ddot{l}_f(t) = F_{a,press}(t) + F_{a,vf}(t) + F_{a,sc}(t) - F_{fs}(t) \quad (2.6)$$

At last, some backlash  $L_b$  probably occur in the attachment between the fork and the sleeve. This parameter is uncertain, but assuming that it is small, it can be approximated as a variable offset error in the output signal  $y_1(t)$ . The output signal can then be described as

$$y_1(t) = l_f(t) + \text{sign}(\dot{l}_f(t) - \dot{l}_s(t)) \frac{L_b}{2} \quad (2.7)$$

The sensor resolution is known and taken from [6].

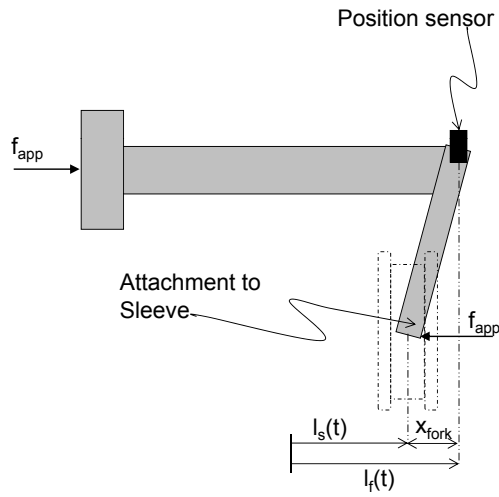


**Figure 2.4.** Displacement between fork and sleeve. Note that the inclination of the fork arm is exaggerated to illustrate the effect. In this case, the velocity of both the fork and the sleeve is zero.

## 2.2 Synchronizer

A synchronizer is a complex mechanism often referred to as a myth and black magic [8]. Different kinds exist, but the most commonly used and the type treated in this thesis, is the strut-type blocking synchronizer. Readers are recommended [8] and [9] for detailed information about transmission synchronizers. This section only treats the main behaviour of a synchronizer in a control perspective.

In figure 2.5, a cutaway view of a typical double cone strut-type blocking synchronizer is shown. The hub and sleeve in the center of the figure are fixed to the input shaft and the sleeve can slide in axial direction. The object of the synchronization process is to move the sleeve through the blocker ring and gear wheel teeth, so it is locked to the gear wheel. A gear wheel can be seen in figure 2.6 and is placed after the inner rings in figure 2.5 (at both sides). The struts are placed between the hub and the sleeve for two reasons. One is to presynchronize the blocker ring to its correct position relative to the sleeve [8]. This action also cause a pressure between the friction rings (the blocker, intermediate and inner rings are in this thesis often mentioned as the friction rings) which wipes the oil between them [8] and enables the friction effects, which is the other purpose with using struts.

The main synchronization takes place after the presynchronization. When a force is applied at the blocker ring it causes a pressure between the three rings which in turn generates the torque required to accelerate/decelerate the input shaft. This torque occurs because of that the blocker and inner rings are fixed to the input shaft and the intermediate ring is fixed to the output shaft (see figure 2.5 and 2.6). Both the inner and outer layer of the intermediate ring is made of a special material which causes a large magnitude of friction. Synchronizers with one, two and three friction surfaces exist and the choice of the number of friction surfaces is a matter of wear and efficiency. Figure 2.7 shows a profile view of the synchronizer mechanism and the gear wheel. Take a moment to study this figure. The interval which involves the synchronization process start at the neutral position (5 in figure 2.7) and ends somewhere beyond the end of the dogging position (8 in figure 2.7). While the real synchronization takes place, the sleeve teeth is in contact with the blocker ring teeth.

When the sleeve teeth moves beyond the blocker ring teeth, it will meet the gear wheel teeth. In this position, the input shaft needs to be turned aside so the sleeve teeth and splines can mesh with the gear wheel splines. Due to the geometry, an axial resistance force will occur, which is even greater if there is any drag at the input shaft (from friction or clutch torque). These forces are called dogging forces or dogging effects.

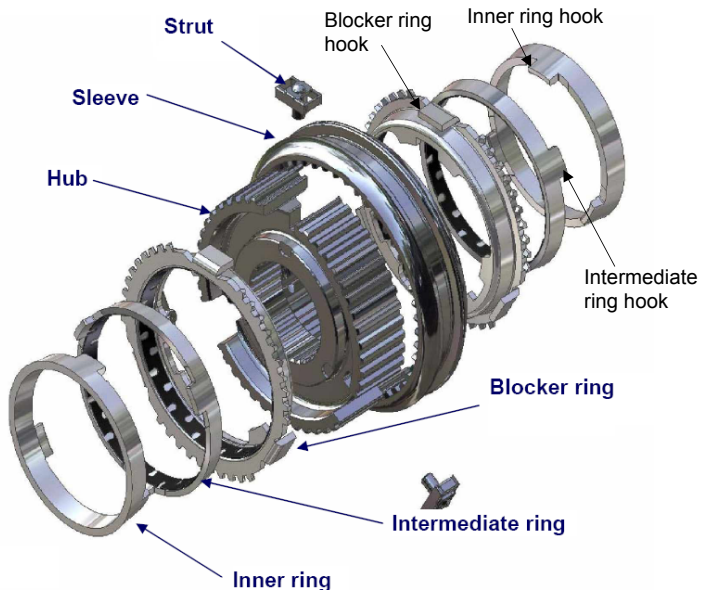


**Figure 2.5.** A cutaway view of a manual transmission synchronizer (taken from internal GMPT documentations). Note the marked hooks at the friction rings. The one at the intermediate ring is hooked into the hole in the gear wheel in figure 2.6 and the hooks at the blocker and inner rings are hooked into holes at the hub.



**Figure 2.6.** A gear wheel. Gear wheels are placed at the ends of the parts in figure 2.5. The intermediate ring hooks in figure 2.5 are hooked into the holes marked in this figure.

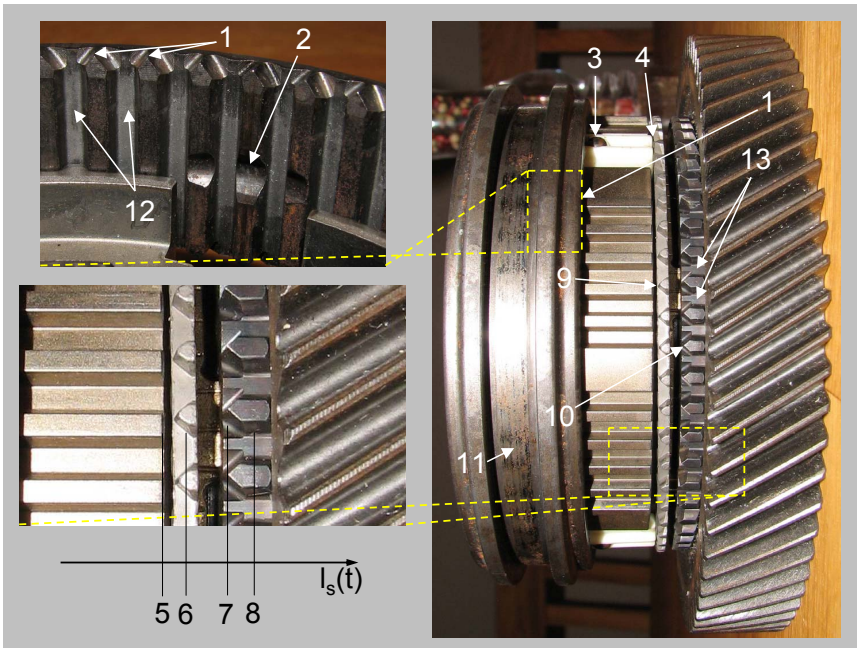


**Figure 2.7.** A profile view of the synchronizer parts. 1) sleeve teeth (when positions are mentioned here, it is referred to this point), 2) sleeve groove (causing a detent force), 3) detent metal ball in strut (attached to a spring inside the strut), 4) strut pressed against the blocker ring (presynchronization), 5) neutral position  $l_{neutral}$ , 6) synchronization position  $l_{synch}$ , 7) position where dogging effects begin in worst case  $l_{dogg,start}$ , 8) position where dogging effects cease  $l_{dogg,end}$ , 9) blocker ring tooth, 10) gear wheel tooth, 11) actuator fork attachment, 12) sleeve splines, 13) gear wheel splines. Note that the upper left picture shows the inside of (the sleeve) the marked area in the right picture.

### 2.2.1 The Synchronizer Sleeve

When moving the the synchronizer sleeve from neutral position (position 5 in figure 2.7) to the engaged position (after position 8 in figure 2.7), some different forces acts on it. The forces propagating on the sleeve are clarified one by one here. First of all the force between the fork and sleeve,  $F_{fs}(t)$  in equation 2.5, must act with opposite sign on the sleeve.

Some dynamic friction may occur. A parameter value  $\mu_{s,df}$  is used, though it is only a guess. According to [10],  $\mu_{s,df}$  is probably smaller than the viscous effects of the actuator system. The equation of the dynamic friction is

$$F_{s,df}(t) = -\mu_{s,df}\dot{l}_s(t) \quad (2.8)$$

where index *df* means dynamic friction.

At the synchronization position  $l_{synch}$  ( 6 in figure 2.7), a force propagates on the sleeve which prevents it to move beyond this position. This force occurs only when there is a difference in angular velocity between the sleeve and the gear wheel (i.e. when there is a slip between the input and output shafts). A detailed explanation of this effect is given in [8]. We only treat this as when there is a difference in angular velocity, the sleeve cannot be moved further and we can state the equation of the synchronization force as

$$F_{s,s}(t) = \begin{cases} \max(0, F_{s,r}(t)) & \text{if } \omega_s(t) \neq 0 \text{ and } l_s(t) = l_{synch} \\ \min(0, F_{s,r}(t)) & \text{if } \omega_s(t) \neq 0 \text{ and } l_s(t) = -l_{synch} \\ 0 & \text{else} \end{cases} \quad (2.9)$$

where  $F_{s,r}$  is the sum of all other forces acting on the sleeve. It should be mentioned here that the sleeve velocity is almost discontinuously changing to zero at the synchronization position and equation 2.9 yields only together with the fact that the sleeve velocity is decreased to zero instantaneously in this point. This is handled by switching between two controllers in the control software when the sleeve is in synchronization position (see chapter 4).

To prevent vibrations and other forces affecting the sleeve when there is no actuator force applied, a detent force is used. It causes the sleeve to move to neutral or engaged position, depending on the sleeve position. Figure 2.8 shows the detent force profile used in this thesis, which is provided by [10]. It is produced by a metal ball pressed by a spring against a groove in the moving surface. In this case a metal ball is placed inside the struts and the grooves are inside the sleeve. An example of this is showed in the little upper right box in figure 2.8 and figure 2.7 shows the metal ball and the grooves of a manual transmission synchronizer. Its behaviour mainly depends on the angles of the groove and the spring rate. The magnitude and profile of the detent force is uncertain and should be calibrated. Because of the nonlinear behaviour of the detent force, it is only described as

$$F_{s,det}(t) = f(l_s(t)) \quad (2.10)$$

A calibrated table of values can be used together with the sleeve position to get the actual detent force.

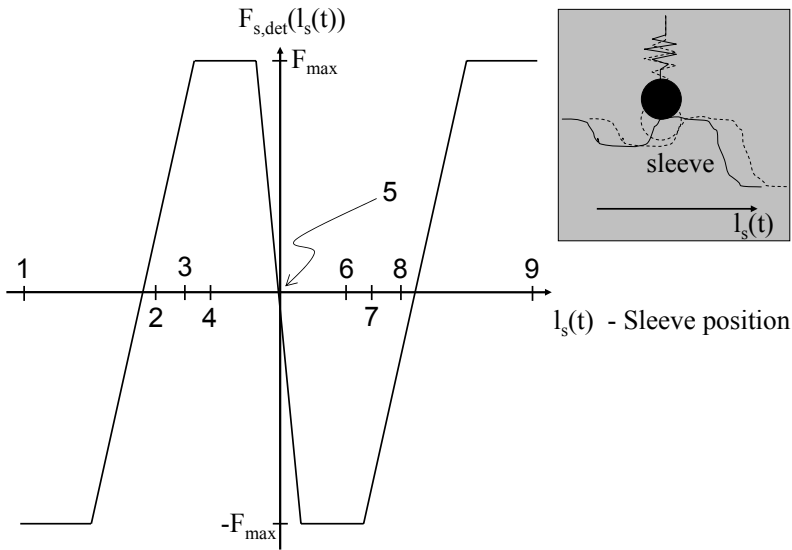


**Figure 2.8.** The figure shows a detent force profile. The sleeve positions marked in the figure are: 1) *Sleeve endstop negative side*, 2)  $-l_{dogg,end}$ , 3)  $-l_{dogg,start}$ , 4)  $-l_{synch}$ , 5)  $l_{neutral} = 0$ , 6)  $l_{synch}$ , 7)  $l_{dogg,start}$ , 8)  $l_{dogg,end}$  and 9) *Sleeve endstop positive side*. A constant increase of the detent force from negative to positive value, combined with system delay and fork position measurements instead of the sleeve position, result in that a smooth movement of the sleeve is difficult to attain. More on this in chapter 4 *Controller implementation* and 5 *Results*. Note that the detent force propagates in a manner which accelerates the sleeve in the direction of neutral position in an interval close to neutral, and towards the end positions in an interval close to them. The little box in upper right corner shows how the metal ball inside the strut is pressed against grooves inside the sleeve. This is what generates a detent force.

After the real synchronization is finished, the blocker ring has to be pulled aside. When a force is applied, a torque occurs due to the geometry of the sleeve and blocker ring teeth. According to [10], the required torque getting the blocker ring to turn aside should not be large enough to affect the synchronization performance since it is, at the most, three friction rings that needs to be turned aside and not the whole input shaft. For more about the details, readers are once again referred to [8] and [9].

Before fully synchronization, the sleeve splines have to mesh with the gear wheel splines. When the sleeve teeth moves beyond the position of the gear wheel teeth  $l_{dogg,start}$ , the angle of the gear wheel is unknown, and treated as random. If the difference between the angle of the gear wheel and the sleeve is not an integer number of an exact angle (dependent on the spline width, the teeth width and the number of splines), the teeth will hit each other and a dogging force will arise. See figure 2.9 for some different examples. To overcome this dogging force, the input shaft has to be accelerated. The dogging force is difficult to calculate, and is related to the sleeve velocity and possible appeared slip after the sleeve has left the synchronization position. Furthermore, a torque transfer in the clutch will strengthen the dogging force even more (it is the dogging effects between the gear wheel and the sleeve teeth that cause the sound when the clutch is engaged too early during a gear shift in a manual transmission). Hence, the dogging force is treated as a disturbance in a specific interval of the sleeve position. If  $\lambda(t)$  is a random number between 0 and 1 the dogging effects will start at

$$\tilde{l}_{dogg,start}(t) = l_{dogg,start} + \lambda(t) (l_{dogg,end} - l_{dogg,start}) \quad (2.11)$$

The dogging force then occur as

$$F_{s,dogg}(t) = \begin{cases} f(\dot{l}_s, l_s, \omega_s) & \text{if } \tilde{l}_{dogg,start}(t) \leq l_s(t) < l_{dogg,end} \\ 0 & \text{else} \end{cases} \quad (2.12)$$

The equation of motion of the sleeve can now be depicted as

$$m_s \ddot{l}_s(t) = F_{fs}(t) + F_{s,df}(t) - F_{s,s}(t) + F_{s,det}(t) + F_{s,dogg}(t) \quad (2.13)$$

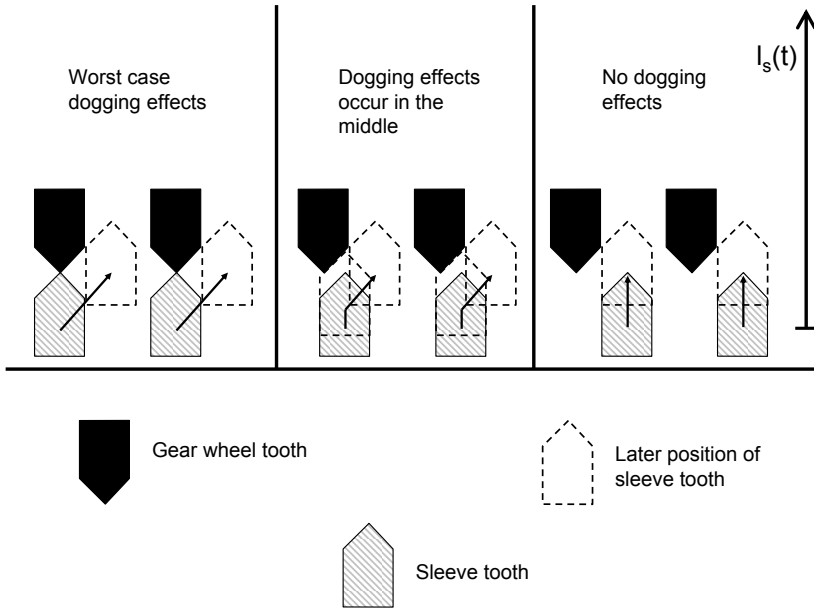


**Figure 2.9.** A schematic view for different gear wheel angles at the moment the sleeve teeth passes gear wheel teeth point. The left picture shows maximum dogging effects, the middle one "intermediate" dogging effects and the right picture shows the case where no dogging effects occur. One can here see how the sleeve has to be turned aside if the teeth positions is not the case as in the right picture. If there is a torque at the input shaft, the sleeve may even bounce backward or between the gear wheel teeth.

### 2.2.2 The Synchronizer Friction Rings

The friction rings (the blocker, intermediate and inner rings) in the synchronizer are the parts which produces the torque needed to synchronize the input and output shafts. In figure 2.5 an example of a synchronizer with two friction surfaces was shown. Here is the friction surface at the inner and outer side of the intermediate ring and a force between the rings produces a torque with the opposite sign as the slip. The slip is calculated as

$$\omega_s(t) = \omega_i(t) + i\omega_o(t) \quad (2.14)$$

where  $i$  is the gear ratio of the actual gear and  $\omega_o(t)$  is negative when driving in forward direction. Figure 2.10 shows a schematic view of how the rings are connected to each other. The angle  $\theta_{cone}$  of the rings is of crucial importance for the behaviour of the synchronization [9]. According to [8], an axial applied force  $F_{s,s}(t)$  on the blocker ring results in a torque  $M_a(t)$  acting on the input shaft which can be calculated as

$$M_a(t) = \frac{r_m \mu_{cone} n_r \text{sign}(-\omega_s(t))}{\sin \theta_{cone}} \text{sign}(F_{s,s}(t)) F_{s,s}(t) \quad (2.15)$$

where  $r_m$  is the mean radius of the friction surfaces,  $n_r$  is the number of friction surfaces and  $\mu_{cone}$  is the friction coefficient. The factor  $\text{sign}(-\omega_s(t))$  can be explained by the fact that if the slip is negative, an acceleration of the input shaft occurs and vice versa. The factor  $\text{sign}(F_{s,s}(t))$  is explained of that the synchronization force is negative at the negative side of the gear gate and positive at the positive side which is needed to get the equation 2.13 correct. But when using the synchronization force to calculate the applied torque, the rate of it is desired. Note here that  $\frac{\mu_{cone}}{\sin \theta_{cone}} < 1$ .

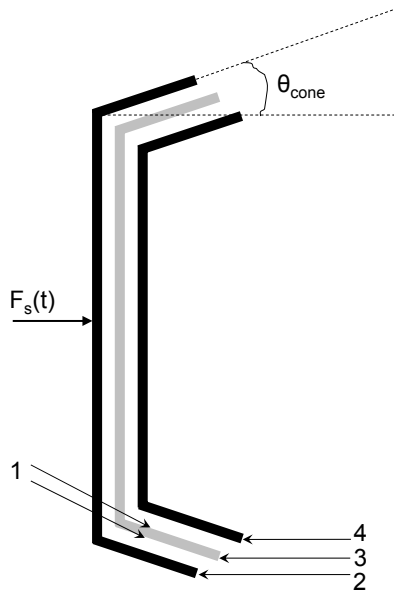


**Figure 2.10.** A schematic view of the friction rings. The angle  $\theta_{cone}$  is of crucial importance for the behaviour of the generation of synchronization torque. The figure shows the friction rings of a double cone synchronizer meaning that there are two friction surfaces, which are at both sides of the intermediate ring pointed out by (1). (2) – (4) shows the blocker, intermediate and inner ring respectively.

## 2.3 The Input and Output Shafts

As mentioned before, the synchronizers are placed at the input shafts in this work. Therefore, the torque from the synchronizer friction rings propagates directly on the shaft which is being accelerated or decelerated. (In the opposite case, the applied torque from the friction rings should be multiplied with the gear ratio of the actual gear.) Assuming that there are no torque transfer in the clutch, there are still some drag at the input shaft. The main part of this drag is temperature dependent due to the viscosity of the oil in the gear box according to a Matlab script from [7]. This script calculates the drag for a specific temperature and angular velocity of the input shaft. It calculates the drag on the input shaft of an ordinary manual transmission rather than of a specific DCT. The drag is uncertain and should be estimated. The script is used to generate the drag in the simulation plant and the affine approximation below is used in the control software. For more about the approximation, see chapter 4.2.3 *Input shaft drag estimation*. Figure 2.11 shows some results of the script and that an affine relation to the angular velocity of the input shaft can be used to approximate the drag. Different affine relations should be used for different temperatures. The affine approximation of the drag is

$$M_{drag}(t) = k_{drag}(\tau)\omega_i(t) + m_{drag}(\tau) \quad (2.16)$$

where  $\tau$  is the oil temperature.

The equation of rotation of the input shaft follow as

$$J_i\dot{\omega}_i(t) = M_a(t) + M_{drag}(t) \quad (2.17)$$

Finally, the angular velocities of the input and output shaft are available as measurements  $y_2(t)$  and  $y_3(t)$  respectively.

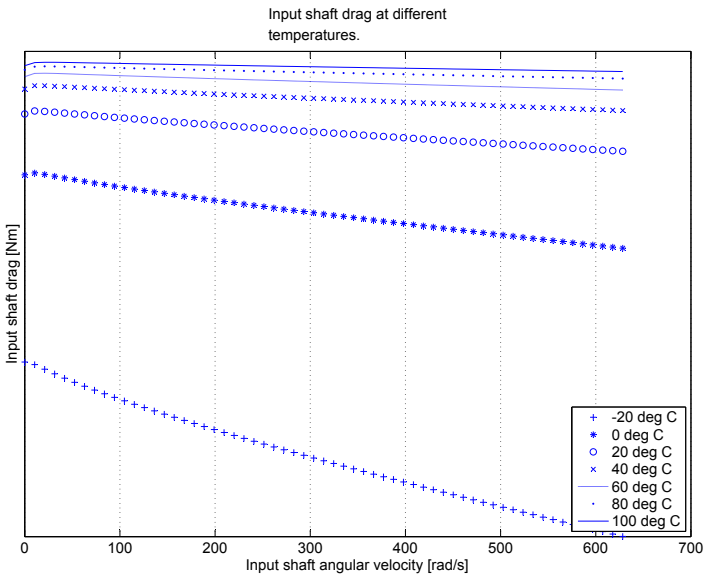


**Figure 2.11.** Some plots of calculated drag at the input shaft for different temperature and input shaft angular velocity. As can be seen, the drag can be well approximated using an affine relation to the angular velocity for a specific temperature. Note that the drag is represented as negative since the angular velocity of the input shaft is positive and the drag is added in the equation of rotation.



# Chapter 3

## System Transfer Function

The control of the synchronization process is divided in two different controllers. One is used when the sleeve is in synchronization position. The control design used for this interval is not a regular model based design and therefore no transfer function is needed. But it can easily be depicted by using the equations of the system in chapter 2.

The other controller is used during transportation of the sleeve. For this interval, a transfer function called the transportation model is depicted.

The idea is to treat the control signal of the system as one requested force  $F_{req}$ , and not two pressure requests. If the pressure of one hydraulic line is controlled active and the other one is held at some pressure  $p_{set} > 0$ , the control signal can be treated as a requested force. Equation 2.2 can be used to describe this as

$$F_{req}(t) = A_1 p_{1req}(t) - A_2 p_{2req}(t) \quad (3.1)$$

This is then used to calculate the pressure of the active line if the held pressure in the other line and the requested force is known.

From here on, frequency domain representation (laplace transform) is used assuming that all initial values are zero. The objective is to depict a transfer function  $G_t(\mathbf{s})$  so that  $Y_1(\mathbf{s}) = G_t(\mathbf{s})\mathbf{F}_{req}(\mathbf{s}) + W_t(\mathbf{s})$ . In  $W_t(\mathbf{s})$  the static and nonlinear terms are collected. Some more steps of the calculations are shown in appendix A *Transfer function calculation*.

Equation 2.1 – 2.2 and 3.1 can be used to describe the force propagating at the fork piston as

$$\mathbf{F}_{req}(\mathbf{s}) = (a_h \mathbf{s} + 1) \mathbf{F}_{a,press}(\mathbf{s}) e^{T_{ad} \mathbf{s}} \quad (3.2)$$

Equation 2.4 – 2.6 can be used to describe the motion of the actuator fork as

$$\begin{aligned} (m_f \mathbf{s}^2 + (c_{fs} + \mu_{a,vf}) \mathbf{s} + k_{fs}) \mathbf{L}_f(\mathbf{s}) = \\ = (c_{fs} \mathbf{s} + k_{fs}) \mathbf{L}_s(\mathbf{s}) + \mathbf{F}_{a,press}(\mathbf{s}) + \mathbf{F}_{a,sc}(\mathbf{s}) \end{aligned} \quad (3.3)$$

The motion of the synchronizer sleeve is finally described using equations 2.5, 2.8 – 2.9 and 2.13

$$(m_s \mathbf{s}^2 + (c_{fs} + \mu_{s,df}) \mathbf{s} + k_{fs}) \mathbf{L}_s(\mathbf{s}) = (c_{fs} \mathbf{s} + k_{fs}) \mathbf{L}_f(\mathbf{s}) + \mathbf{F}_{s,det}(\mathbf{s}) + \mathbf{F}_{s,dogg}(\mathbf{s}) \quad (3.4)$$

Note that the synchronization force  $F_{s,s}$  is zero during transportation and omitted here. If the backlash  $L_b$  in the fork sleeve attachment is omitted, equation 2.7 can be used with 3.2 – 3.4 to get the transfer function of the transportation model

$$G_t(\mathbf{s}) = \frac{(m_s \mathbf{s}^2 + (c_{fs} + \mu_{s,df}) \mathbf{s} + k_{fs})}{(a_h \mathbf{s} + 1) A_t(\mathbf{s})} e^{-T_{ad} \mathbf{s}} \quad (3.5)$$

$$A_t(\mathbf{s}) = \mathbf{s} (m_f m_s \mathbf{s}^3 + (c_{fs}(m_f + m_s) + m_f \mu_{s,df} + m_s \mu_{a,vf}) \mathbf{s}^2 + (k_{fs}(m_s + m_f) + c_{fs}(\mu_{a,vf} + \mu_{s,df}) + \mu_{s,df} \mu_{a,vf}) \mathbf{s} + k_{fs}(\mu_{a,vf} + \mu_{s,df}))$$

where  $A_t$  is used instead of a A1 format paper. The nonlinear terms affects the system as

$$W_t(\mathbf{s}) = \frac{(c_{fs} \mathbf{s} + k_{fs})}{A_t(\mathbf{s})} (\mathbf{F}_{s,det}(\mathbf{s}) + \mathbf{F}_{s,dogg}(\mathbf{s})) + \frac{m_s \mathbf{s} + (c_{fs} + \mu_{s,df}) \mathbf{s} + k_{fs}}{A_t(\mathbf{s})} \mathbf{F}_{a,sc}(\mathbf{s}) \quad (3.6)$$

# Chapter 4

## Controller Implementation

The control software is implemented in Simulink and tested on the simulation plant from GMPT. The simulation plant is slightly extended to be able to represent the phenomenons of interest in this thesis. The model simulates only one gear gate and therefore only two gears, mentioned as gear  $g_p$  in positive direction of the gear gate and  $g_n$  in negative direction. The control delay  $T_{cd}$  is assumed to be one sample ( $T_s$ ). Figure 4.1 shows how the to level of the control system is designed.

Due to the difference in the transportation interval and the synchronization interval, the process needs to be split up in at least three intervals: before synchronization, synchronization and after synchronization. In fact, the process is split up in four different intervals. The interval after the synchronization is divided in two parts – after synchronization and engaging. This enables a slow enclosure of a position between the synchronization position and the endstop, preferable the dogging position  $l_{dogg,start}$ . Furthermore, it leaves possibilities to change controller or control parameters.

The control sequence is divided into four steps. The two middle steps are estimations followed by controllers calculating the requested actuator force. The estimations are made in a block called *Observer*. It handles prediction of the fork position because of delay in the system, detent and static/coulomb friction force estimations and also input shaft drag estimation. The *Controller* block consists of PID and manual controllers (it is called manual because of that no regular model based design is used) which are based on the process model  $G_t(\mathbf{s})$  and the equations of the input shaft rotation.

The chosen way of controlling the actuator force is to actively control the pressure of one line every sample while a constant pressure is held at the other line. Referred to figure 2.3, the hydraulic line one is preferred as the active line during engagement of the gear in positive direction and to be the idle line during engagement of the gear in negative direction. The pressures are calculated in a block called *Pressure Calculation*. Compensation of the static and nonlinear detent and friction forces, as well as for the input shaft drag, is also made in this block.

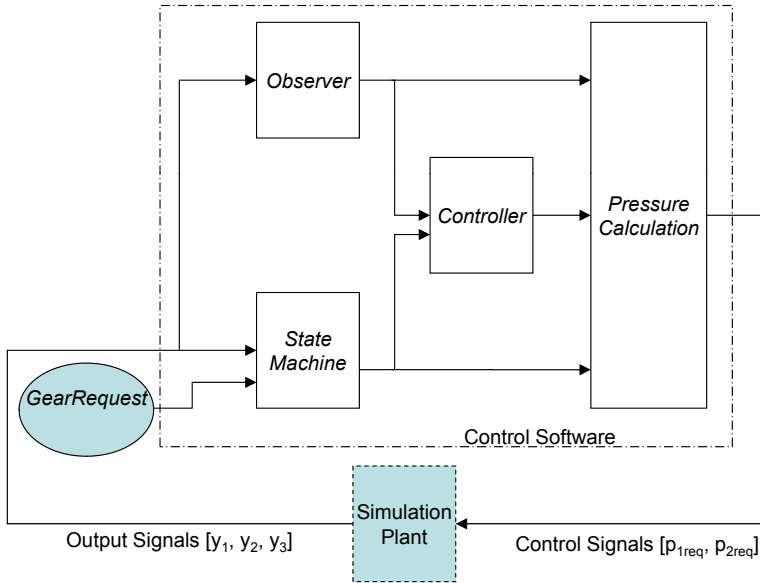


**Figure 4.1.** This figure shows the signal flow of the *Control Software*. The main control signal calculation is made in the *Controller* block. The *State Machine* is a central part and it handles the calculations of idle pressure, reference signals, control parameters and which controller that should be used.

To be able to switch between different controllers, use different control parameters, calculate reference signals and calculate idle pressure, a *State machine* block is used. It is implemented in Stateflow and is a central part of the control software.

In table 4.1, the input and output signals are listed. Following sections explain the four different blocks and every section starts with a similar table of signals for the actual block.

---

<b>Signal</b>	<b>Type</b>	<b>Description</b>
$GearRequest$	Input	Requested gear which in real case is an input from some other control software. $GearRequest \in [0, g_p, g_n]$
$y_1(t)$	Input	Fork position $l_f(t)$ . Output one of the simulation plant.
$y_2(t)$	Input	Input shaft angular velocity $\omega_i(t)$ . Output two of the simulation plant.
$y_3(t)$	Input	Output shaft angular velocity $\omega_o(t)$ . Output three of the simulation plant.
$p_{1req}(t)$	Output	Requested pressure of hydraulic line one.
$p_{2req}(t)$	Output	Requested pressure of hydraulic line two.

**Table 4.1.** Table of inputs and outputs of the *Control Software*.

## 4.1 State Machine

The purpose of the state machine is to switch actual controller and control parameters. Moreover it calculates reference signals and desired idle pressure. The actual state is saved in the variable *State*, and the states correspond to either a specific interval in the process, synchronization positions, neutral position or engaged positions. Figure 4.2 shows these state relations to fork position. The states (1) – (4) corresponds to the intervals *before synchronization*, *synchronization*, *after synchronization* and *engagement*. There are also negative counterparts of these states which corresponds to the same intervals in negative fork direction. Both directions share the states *engaged* (5) and *disengaging* (10).

In every state, there are some function calls. A description of these functions and a flowchart of the state machine can be found in appendix C. One of the functions enables that an integration part can be added in the position controller after a user specified time. The linear transportation model in equation 3.5 includes an integration and a PD controller seems to be a good choice. Though, because of the static friction and detent forces, a not negligible static error occur in some cases when using a PD controller. In those cases an integration part is desired, even if it results in a not as smooth control as desired. The idea is then: try to get a smooth control with a PD controller and if the fork position get stuck in wrong place, add an integration part. The time of when the integration part is included is set individually for every state. This will also solve the problem if a transition to the state *after synchronization* occur before synchronization is finished. It may be very hard to find out a specific magnitude of the slip of which the blocker release occur, and in reality there are probably some noise affecting the shaft angular velocity signals. Moreover, the behaviour of the synchronization torque during the final decrease of the slip may not be as linear as in equation 2.15 (compare this with the behaviour of a car the last meters before stop when the brakes are pressed hard). Simulations shows that the applied force, using a PD controller in the case of a too early transition to state *after synchronization* and a significant amount of input shaft drag, is too small to synchronize the input and output shafts. The fork and sleeve is then stuck in the synchronization position and the rate of the slip is increasing. This problem only occur if the slip is negative (i.e. acceleration of the input shaft), otherwise the drag would rather help. An integration part solves this problem.

Another function switches the boolean variable *StateShift* between *false* and *true* and the condition of which it is set as *true* is explained in table C.1. This boolean is used as the test in transition between several states.

Signal	Type	Description
<i>GearRequest</i>	Input	Requested gear. $GearRequest \in [0, g_p, g_n]$ .
$y_1(t)$	Input	Fork position $l_f(t)$ . Output one of the simulation plant.
$y_2(t)$	Input	Input shaft angular velocity $\omega_i(t)$ . Output two of the simulation plant.
$y_3(t)$	Input	Output shaft angular velocity $\omega_o(t)$ . Output three of the simulation plant.
$F_{req}(t - T_s)$	Input	Last sample requested force from the controller.
<i>PositionReference</i>	Output	Fork position reference.
<i>RotSpeedReference</i>	Output	Input shaft angular velocity reference.
<i>ControllerSwitch</i>	Output	This signal enables switching between transportation, synchronization and no controller in the controller block.
<i>ControllerTenable</i>	Output	Enable transportation controller. Used to reset the integration part.
<i>ControllerSenable</i>	Output	Enable of synchronization controller. Used to detect first sample of state $\pm 2$ to get a smooth switch from transportation controller.
<i>ControllerParams</i>	Output	Includes a vector with PID parameters $[K, K_i, K_d]$ . This enables different parameter values in different intervals.
<i>BackPressure</i>	Output	Requested idle pressure at the idle hydraulic line.
<i>State</i>	Output	Actual state in the state machine.

**Table 4.2.** Table of inputs and outputs in the *State Machine* block.

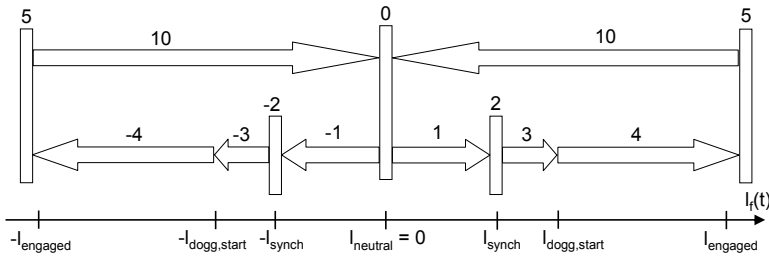


**Figure 4.2.** This figure shows the connections between *State* and the fork position. State  $\pm 2$  is the synchronization state. A transition to state  $\pm 3$  occurs when the magnitude of the slip is less than a user specified value  $d\omega$ . In state 0, the *GearRequest* is 0. The names of the states are 0) *Neutral*,  $\pm 1$ ) *Before Synchronization*,  $\pm 2$ ) *Synchronization*,  $\pm 3$ ) *After Synchronization*,  $\pm 4$ ) *Engaging*, 5) *Engaged* and 10) *Disengaging*. The position of transition between state *After Synchronization* and *Engaging* can easily be changed if no slow enclosure of the dogging position is wanted.

Signal	Type	Description
$y_1(t)$	Input	Fork position $l_f(t)$ . Output one of the simulation plant.
$y_2(t)$	Input	Input shaft angular velocity $\omega_i(t)$ . Output two of the simulation plant.
$y_3(t)$	Input	Output shaft angular velocity $\omega_o(t)$ . Output three of the simulation plant.
$p_{1req}(t - T_s)$	Input	Last sample requested pressure of pressure line one from the <i>Pressure Calculation</i> block.
$p_{2req}(t - T_s)$	Input	Last sample requested pressure of pressure line two from the <i>Pressure Calculation</i> block.
<i>PositionPrediction</i>	Output	Fork position estimation.
<i>DetentEstimation</i>	Output	Detent force estimation.
<i>ForkFrictionEstimation</i>	Output	Static and coulomb force estimation.
<i>DragEstimation</i>	Output	Estimation of the drag torque affecting the input shaft.

**Table 4.3.** Table of inputs and outputs in the *Observer* block.

## 4.2 Observer

In the *Observer* block, some variables are predicted and estimated. Fork position prediction is desired because of the delay between the control software and the hydraulic pressure. Estimations of the detent and static/coulomb friction forces and the input shaft drag are needed to enable compensation. The fork position prediction can be used as input signal in the controller block and to estimate the detent force. The gear box oil temperature is assumed to be available and is used to estimate the input shaft drag, which is used with the other estimations in *Pressure calculation* for compensation. Table 4.3 shows the input and output signals of the block.

### 4.2.1 Fork Velocity and Position Prediction

A simple model of the fork and sleeve for the transportation interval is used and the spring and damper effects between them are omitted. If the position of the total mass of the fork and the sleeve is denoted as  $l_o(t)$ , following equation of motion can be derived using equations 2.6 and 2.13

$$(m_f + m_s)\ddot{l}_o(t) = F_{a,press}(t) + F_{a,vf}(t) + F_{s,df}(t) + F_{s,det}(t) + F_{a,sc}(t) \quad (4.1)$$

where the dogging force in equation 2.13 is omitted. The dynamics in the hydraulic system is assumed to be negligible, since the time constant  $a_h$  is smaller than the sample time. The equations 2.1, 2.4, and 2.8 can then be used in equation 4.1 to derive the discrete approximation of the acceleration of the mass of the fork and sleeve

$$\begin{aligned} \ddot{l}_o(k) &= \\ \frac{1}{m_f + m_s} & (A_1 p_{1req}(k-n) - A_2 p_{2req}(k-n) - (\mu_{a,vf} + \mu_{s,df}) \dot{l}_o(k) + F_{a,sc}(k) + F_{s,det}(k)) \\ &= F_\Sigma(k) \end{aligned} \quad (4.2)$$

where  $n$  is the integer  $n = \text{round}\left(\frac{T_{ad}}{T_s}\right)$ . The static/coulomb friction and detent force can be used from the estimations in section 4.2.2. A prediction of the velocity one sample ahead is approximated as

$$\dot{l}_o(k+1) = \dot{l}_o(k) + F_\Sigma(k)T_s \quad (4.3)$$

This is used to predict the position one sample ahead as

$$\begin{aligned} l_o(k+1) &= l_o(k) + \left( \dot{l}_o(k) + \frac{\dot{l}_o(k+1) - \dot{l}_o(k)}{2} \right) T_s = \\ &= l_o(k) + T_s \dot{l}_o(k) + \frac{T_s^2}{2} F_\Sigma(k) \end{aligned} \quad (4.4)$$

This can be iterated and the values of  $p_{1req}(k-i)$  and  $p_{2req}(k-i)$  where  $i = 0, 1, \dots, n$  is available if the pressure requests are stored internal in the controller software. The velocity used in the first iteration is calculated using euler backward approximation as

$$\dot{l}_o(k) = \frac{l_f(k) - l_f(k-1)}{T_s} \quad (4.5)$$

There is a manual switch used when no prediction is wanted (the measurement  $y_1(k)$  is set as the output *PositionPrediction*). The prediction only works satisfying in some cases and therefore no prediction is normally used. But there is a great interest in predicting the position and that is why this work is not discarded. The transportation controller, presented in section 4.3.1, is based on the case when no prediction is made and in that case the position prediction is simply the actual fork position.

### 4.2.2 Detent and Static/Coulomb Friction Estimation

The detent force of time  $k + j, j = 0, 1, \dots, n$  is estimated by using the positions of section 4.2.1 as input to a look-up table of the detent force profile. The static/coulomb friction are estimated by using the positions and velocities of section 4.2.1 in equation 2.3.

### 4.2.3 Input Shaft Drag Estimation

A review of figure 2.11 shows that the input shaft drag can be approximated with an affine relation to the angular velocity for a specific temperature. An estimation of  $k_{drag}$  and  $m_{drag}$  coefficients in equation 2.16 is made by using the method of least square [1]. This is made for different temperatures and the solid lines in figure 4.3 shows the calculated coefficients in relation to the temperature. Next step is to estimate the relation between the coefficients and the temperature using a fourth order function:

$$\begin{aligned} k(\tau) &= c_{k4}\tau^4 + c_{k3}\tau^3 + c_{k2}\tau^2 + c_{k1}\tau + c_{k0} \\ m(\tau) &= c_{m4}\tau^4 + c_{m3}\tau^3 + c_{m2}\tau^2 + c_{m1}\tau + c_{m0} \end{aligned} \quad (4.6)$$

This is also performed by using the method of least square. The resulting approximation of  $k_{drag}$  and  $m_{drag}$  is plotted with stars in figure 4.3. One may think that a second order relation should be good enough, but tests show that the approximated drag then increases for the higher temperatures (i.e. the maximum of the second order approximation occur at a temperature well below 100 degree Celsius). Finally, the right plot in figure 4.4 shows the approximated drag for different temperatures. The estimated coefficients in equation 4.6 are used in equation 2.16, which result in the following estimation of the input shaft drag

$$\begin{aligned} M_{drag}(t) &= \\ & (c_{k4} + c_{k3}\tau^3 + c_{k2}\tau^2 + c_{k1}\tau + c_{k0}) \omega_i(t) + c_{m4} + c_{m3}\tau^3 + c_{m2}\tau^2 + c_{m1}\tau + c_{m0} \end{aligned} \quad (4.7)$$

This method may be used, together with measurements of the drag and oil temperature, to calibrate a drag approximation.

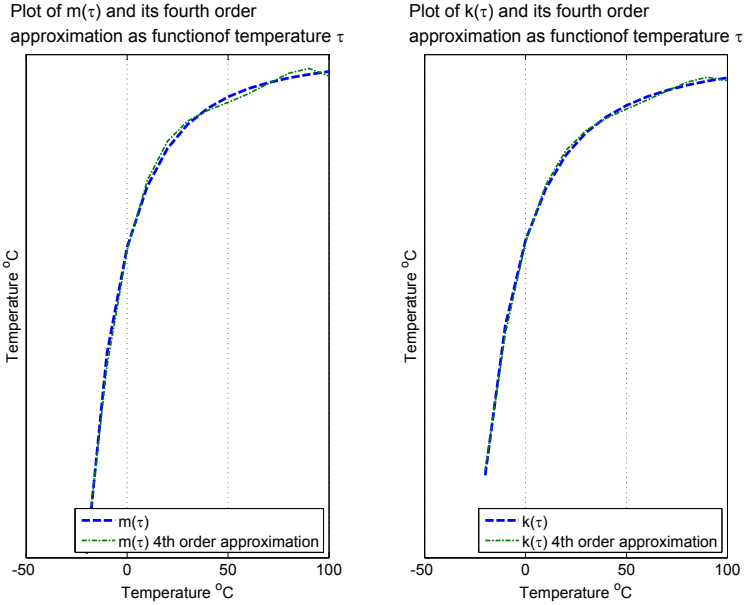


**Figure 4.3.** A plot of the estimated drag coefficients 2.16 in relation to the temperature. It also shows the estimation of a fourth order polynomial between the estimated coefficients and the temperature. The magnitude of the  $m$ -values are much larger than the  $k$ -values. Compare this to the fact that the static drag is greater than the angular velocity dependent drag as can be seen in figure 2.11.

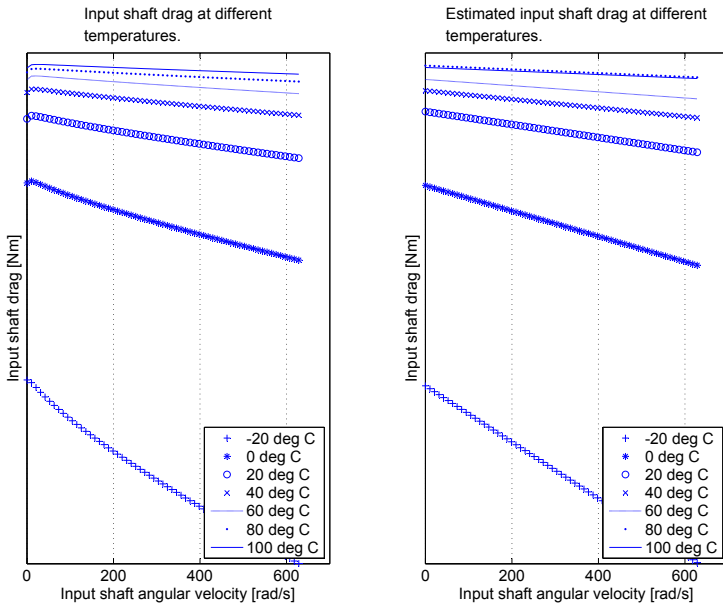


**Figure 4.4.** The right plot shows the estimated input shaft drag as a function of angular velocity, while the left plot shows the "real" values.

### 4.3 Controller

This block consist of one subsystem for the transportation interval, one for the synchronization interval and one switch. The requested force output of the switch is zero when the input *ControllerSwitch* is zero. If *ControllerSwitch* is one, the output force request is the output of the transportation block, and if it is two the controller block output is the output of the synchronization block. The transportation subsystem is a PID controller and the synchronization subsystem contain a PID controller and a manual controller, where the user can switch between the two kinds of controllers. Instead of a table of signals for this block, the subsections of the two intervals contain their own tables of signals.

Signal	Type	Description
<i>PositionReference</i>	Input	Fork position reference signal.
<i>PositionPrediction</i>	Input	Fork position prediction. Normally it is $y_1(t)$ but the user can manually choose it to be the prediction presented in chapter 4.2.1 <i>Fork velocity and position prediction</i> .
<i>ControlParams</i>	Input	PID parameters $K$ , $K_i$ and $K_d$ used in the controller.
<i>ControllerTenable</i>	Input	Used to enable the PID controller and to reset the integration part when it is not used.
$u_t(t)$	Output	Output signal of the controller (requested actuator force).

**Table 4.4.** Table of inputs and outputs in the transportation model part of the *Controller* block.

### 4.3.1 Transportation

A PID controller is used to control the requested force in the transportation intervals (state  $\pm 1, \pm 3, \pm 4, 10$ ) and the control variable is the fork position. Table 4.4 shows the table of input and output signals of this block.

The used PID controller is

$$\mathbf{U}_t(\mathbf{s}) = K \overbrace{\left( 1 + \frac{K_i}{\mathbf{s}} + K_d \mathbf{s} \right)}^{F_t(\mathbf{s})} \mathbf{E}(\mathbf{s}) \quad (4.8)$$

where  $\mathbf{E}(\mathbf{s})$  is the fork position error  $PositionReference - \mathbf{L}_f(\mathbf{s})$ . Figure 4.5 shows the configuration of the system. A step response of the transportation model in equation 3.5 shows that it can be approximated with a *Ziegler-Nichols* model [3] as in equation 4.9 below, where  $b$  is the slope of the step response and  $L$  is the total time delay from control system to hydraulic pressure.

$$\begin{aligned} G_t(\mathbf{s}) &\approx \frac{b}{\mathbf{s}} e^{-sL} \\ L &= T_{ad} + T_{cd} \end{aligned} \quad (4.9)$$

According to Ziegler-Nichols PID tuning table in [3], the parameters should have the values of table 4.5. In the discrete implementation of the controller in equation 4.8, euler approximation of the derivatives [3] is used which result in the discrete

Parameter	Value	Numerical value
$\tilde{K}$	$\frac{1.2}{bL}$	$3.74 \cdot 10^4$
$K_i$	$\frac{1}{2L}$	$1.93 \cdot 10^{-2}$
$K_d$	$\frac{L}{2}$	$4.81 \cdot 10^{-3}$

**Table 4.5.** PID parameter values according to Ziegler-Nichols PID tuning table.  $\tilde{K}$  is used here to separate it from the used gain  $K$  in the controller.

controller

$$\begin{aligned} \mathbf{U}_t(\mathbf{z}) &= K \left( 1 + K_i \frac{1}{\frac{1-\mathbf{z}}{T_s}} + K_d \frac{1-\frac{1}{\mathbf{z}}}{T_s} \right) \mathbf{E}(\mathbf{z}) = \\ &= K \underbrace{\left( 1 + K_i \frac{T_s \mathbf{z}}{\mathbf{z}-1} + K_d \frac{\mathbf{z}-1}{T_s \mathbf{z}} \right)}_{\mathbf{F}_t(\mathbf{z})} \mathbf{E}(\mathbf{z}) \quad (4.10) \end{aligned}$$

Figure 4.6 shows a root locus of the closed loop system where a discrete approximation of  $G_t(\mathbf{s})$  is used. The gain  $K$  in the controller  $F_t(\mathbf{z})$  is the varied feedback and the values of  $T_i$  and  $T_d$  in table 4.5 are used in  $F_t(\mathbf{z})$ . The root locus shows that the gain value  $\tilde{K}$  in table 4.5 is too large. This is because of that the stability margin is decreasing for a discrete approximation. According to the root locus, a maximum value of about  $3.1 \cdot 10^4$  can be used. In some cases and intervals, there is a interest in using a PD controller (see section 4.1 *State Machine*). It shows a larger maximum gain value ( $K \approx 3.5 \cdot 10^4$ ) if the same value of  $K_d$  is used and  $K_i$  is zero. The advantage is a significant decrease of the overshoot. Step responses of a discrete approximation of the closed loop system with PID and PD controllers are shown in figure 4.7. A feedback gain of  $K = 0.3\tilde{K}$  is used for both controllers. Figure 4.8 shows bode plots of the sensitivity functions and complementary sensitivity functions of the closed loop systems when using PID and PD control. To minimize effects of system disturbances, a low magnitude at low frequencies is desired for the sensitivity function [4]. Sensor noise usually occur at higher frequencies and therefore a low magnitude at higher frequencies is desired for the complementary sensitivity function [4]. The bode plot shows that the PD controller is better in respect of this.

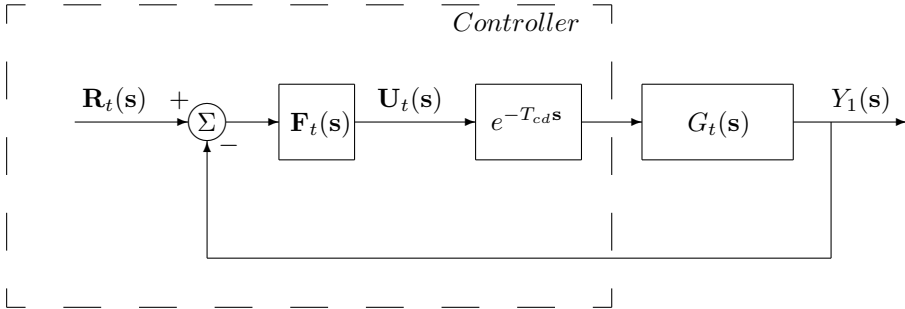


**Figure 4.5.** Signal flow of the system. The controller  $F_t(s)$  takes the fork position error as input. The delay block represent the control delay and the actuator delay is included in the transportation model  $G_t(s)$ .

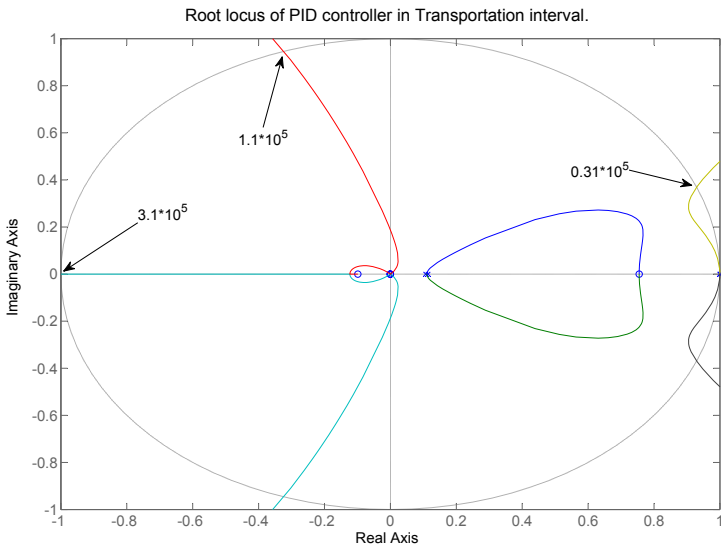


**Figure 4.6.** Root locus of a discrete approximation of the transportation model  $G_t(s)$ , controlled by the PID controller in equation 4.10 with variation of the gain factor  $K$ . It shows that the maximum value of  $K$  which generates a stable system is  $K \approx 3.1 \cdot 10^4$ .

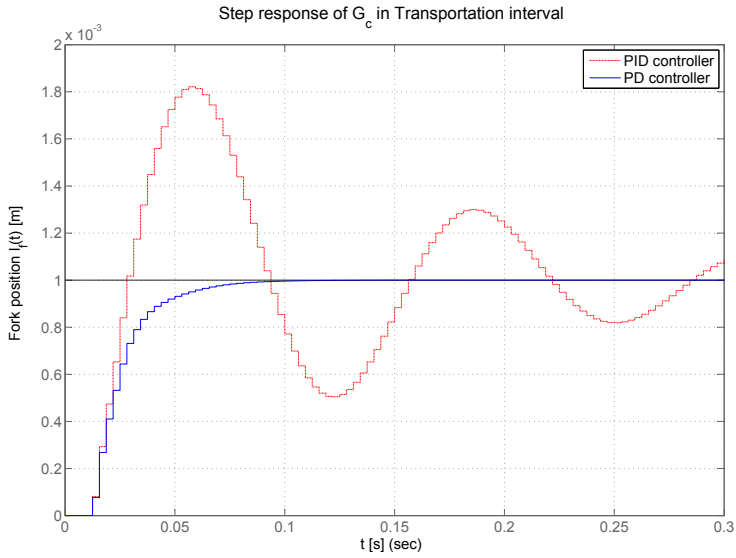


**Figure 4.7.** Step response of the closed loop transportation model system. The signal with a large overshoot is with PID control and the other one is the step response using PD control. A feedback gain  $K = 0.3\bar{K}$  is used with the values of  $K_i$  and  $K_d$  in table 4.5 (only  $K_d$  in the PD controller).

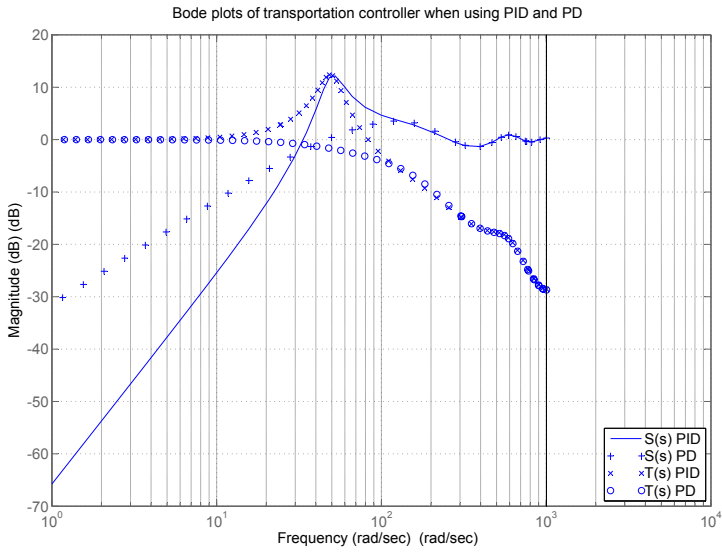


**Figure 4.8.** Bode plot of the sensitivity functions  $S(s)$  and complementary sensitivity functions  $T(s)$  for the closed loop system using the transportation model with PID and PD control.

Signal	Type	Description
<i>RotSpeedReference</i>	Input	Reference value of the input shaft angular velocity.
$y_2(t)$	Input	Input shaft angular velocity.
$u_i(t - T_s), i = s \text{ or } t$	Input	Force request of the last sample. Used as start value in the first sample of the synchronization interval, and to calculate the integrated force $A_-$ . $i = t$ in case of first sample (transportation controller output)
<i>GearRequest</i>	Input	Requested gear. Used to detect if the output force request should be multiplied with $-1$ (synchronization of the gear $g_n$ in negative direction of the gear gate).
<i>ControllerSenable</i>	Input	Used to detect the first sample of the interval.
$u_s(t)$	Output	Output signal of the controller (requested actuator force).

**Table 4.6.** Table of inputs and outputs in the synchronization model part of the *Controller* block.

### 4.3.2 Synchronization

The user can manually switch between PID and manual control in this system. The manual control is more effective and use maximum synchronization force in a great part of the synchronization interval. One may think that a large gain of the PID parameters will do the same. But the problem lies in controlling the applied force in the beginning and in the end of the synchronization. A controlled increase of the synchronization force in the beginning is desired as well as a smooth end of the synchronization. Using PID with large gain values it is hard to obtain these criterion. However, a PID controller is implemented and is possible to use but the focus here is on the manual controller. In table 4.6, the input and output signals of this *Controller* subsystem are listed.

Parameter	Description
$f_0$	Minimum initial value (first sample value)
$f_{ss}$	Force where the ramp slope is switched between $k_{s,Lo}/k_{s,Hi}$ . ( $ss$ = switch slope)
$f_{max}$	Maximum synchronization force used. Should be adjusted so that no pressure saturation occur.
$f_{end}$	End value of the synchronization force.
$k_{s,Lo}$	Desired lower slope of the increase/decrease of the synchronization force.
$k_{s,Hi}$	Desired larger slope of the increase/decrease of the synchronization force.
$\Omega_{end}$	Desired magnitude of the slip when the synchronization force is decreased to the value $f_{end}$

**Table 4.7.** Table of design parameters in the manual synchronization controller. Compare the parameters to figure 4.9.

### Manual Control

The manual controller is developed with the purpose to let the synchronization force  $F_{s,s}$  follow the behaviour shown in figure 4.9. An increase (ramp) with slope  $k_{s,Lo}$  is desired until the force reaches  $f_{ss}$ . Then a larger value  $k_{s,Hi}$  is used until it reaches a specified value of  $f_{max}$  where it is held constant. To enable a smooth switch between the transportation and synchronization controller, the increase should start at the value of the last sample from the transportation controller, if it is larger than  $f_0$ . Otherwise the requested force starts at  $f_0$ . When the pressure of the active hydraulic line reaches its saturation value, the idle pressure is decreased to zero. This enables a significant amount of extra synchronization force. When the pressure of the active line later is decreased, the idle pressure is increased to its earlier value.

A decrease of the synchronization force using the same slopes as the increase is desired. The purpose is to decrease the force to a value  $f_{end}$  before the magnitude of the slip reaches  $\Omega_{end}$ . Consequently, the manual control algorithm includes seven design parameters which are listed in table 4.7.

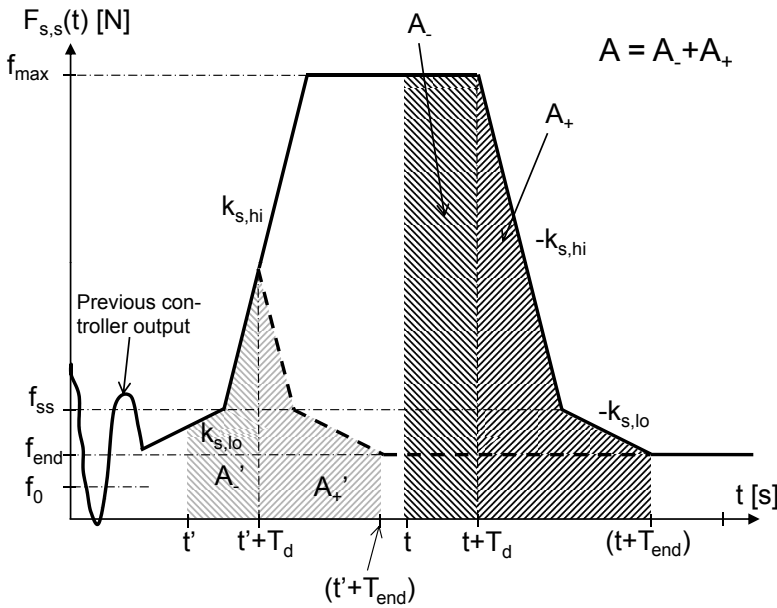


**Figure 4.9.** The figure shows the desired synchronization force. The desired input shaft angular velocity at time  $t + T_{end}$  is  $RotSpeedReference + sign(\omega_s(t))\Omega_{end}$  and the slopes of the curve are  $k_{s,hi}$  and  $k_{s,lo}$ .  $t + T_d$  is the time of when the synchronization force should start to decrease, and it is calculated by using the marked areas in equation 4.11.  $T_d$  is the approximated delay from requested actuator force to synchronization force. Hence,  $t$  is the time of when the force request should start to decrease. The dotted force and areas  $A'_+$  and  $A''_+$  shows the desired synchronization force in a case of low slip at the time of synchronization start. If the magnitude of the slip is large at time  $t'$ , the prediction of the slip at time  $t' + T_{end}$  will be larger than  $\Omega_{end}$  and therefore the increase of the requested actuator force will continue.

This algorithm includes calculation of when the decrease of the force should start. It can be performed by assuming that the decrease of the requested actuator force starts at the actual moment, if it has not already started, and predict if the magnitude of the slip will reach the value of  $\Omega_{end}$  before the synchronization force reaches  $f_{end}$ . If the synchronization force reaches  $f_{end}$  at time  $t + T_{end}$ , and the integrated force from time  $t$  until time  $t + T_{end}$  is known, equations 2.15 and 2.17 can be used to predict  $\omega_i(t + T_{end})$ . The input shaft drag is omitted because of compensation in the pressure calculation block.

$$\begin{aligned}
\dot{\omega}_i(t) &= \frac{r_m n_r \mu_{cone} \text{sign}(-\omega_s(t))}{J_{input} \sin \theta_{cone}} F_{s,s}(t) \implies \\
\implies \int_t^{t+T_{end}} \dot{\omega}_i(t) dt &= \frac{r_m n_r \mu_{cone} \text{sign}(-\omega_s(t))}{J_{input} \sin \theta_{cone}} \int_t^{t+T_{end}} F_{s,s}(t) dt \iff \\
\iff \omega_i(t + T_{end}) - \omega_i(t) &= \frac{r_m n_r \mu_{cone} \text{sign}(-\omega_s(t))}{J_{input} \sin \theta_{cone}} \cdot A \iff \\
\iff \omega_i(t + T_{end}) &= \omega_i(t) - \frac{r_m n_r \mu_{cone} \text{sign}(\omega_s(t))}{J_{input} \sin \theta_{cone}} \cdot A \quad (4.11)
\end{aligned}$$

where  $A$  is the integrated force which can be seen in two different examples in figure 4.9. The test if the magnitude of the slip is smaller or equal to  $\Omega_{end}$  can be translated to a test of the input shaft angular velocity as

$$|\omega_s| \leq \Omega_{end} \iff \begin{cases} \omega_i \geq \text{RotSpeedReference} - \Omega_{end}, & \text{if } \omega_s \leq 0 \\ \omega_i \leq \text{RotSpeedReference} + \Omega_{end}, & \text{if } \omega_s \geq 0 \end{cases} \quad (4.12)$$

since  $\text{RotSpeedReference} = -i\omega_o$  where  $i$  is the actual gear ratio.

To use the calculation in equation 4.11, the integrated force  $A$  is needed. The synchronization force is not measurable, but is approximated as  $F_{s,s}(t) = u_s(t - T_d)$  where  $T_d = T_{ad} + T_{cd} + 10$  ms. The term 10 ms is an approximation of the dynamics from hydraulic pressure to synchronization force.  $u_s$  is the output requested force from this manual controller. This raises a need of knowing the output force request  $T_d$  time backwards. The maximum value, in case of a start of the decrease before the force reaches  $f_{max}$ , is stored as well as a boolean which tells if the decrease has started. This information together with the assumption that a decrease is performed as in figure 4.9, enables calculation of the integrated force as

$$\begin{cases} A = A_- + A_+ \\ A_- = \int_t^{t+T_d} F_{s,s}(t) dt \approx \int_{t-T_d}^t u_s(t) dt \\ A_+ = \int_{t+T_d}^{t+T_{end}} F_{s,s}(t) dt \approx \int_t^{t+T_{end}-T_d} u_s(t) dt \end{cases} \quad (4.13)$$

Two cases of the total integrated force are shown as marked areas in figure 4.9. In the first case, the slip is small when the synchronization starts and the force decrease starts before it reaches  $f_{max}$ .

When a decrease of the requested actuator force is performed, the values of the design parameters are not used directly. The force generating  $A_-$  is already actuated at time  $t$  and impossible to affect. Equation 4.11 can be modified as

$$A = A_- + \tilde{A}_+ = \frac{J_{input} \sin \theta_{cone}}{r_m n_r \mu_{cone} \text{sign}(\omega_s(t))} \left( \omega_i(t) - \underbrace{(\text{RotSpeedReference} + \text{sign}(\omega_s(t)) \Omega_{end})}_{\text{desired } \omega_i(t+T_{end})} \right) \quad (4.14)$$

where  $A_-$  is already calculated.  $\tilde{A}_+$  is the integrated force that is needed to decrease the magnitude of the slip to  $\Omega_{end}$ . A decrease of the synchronization force using the same slopes is still desired. But if  $\tilde{A}_+$  differs from  $\int_t^{t+T_{end}-T_d} u_s(t) dt$ , then the requested force should be corrected to a value that result in the correct integrated force. Figure 4.10 shows an example of when the slip has decreased faster than predicted and  $\tilde{A}_+$  is smaller then the value of  $\int_t^{t+T_{end}-T_d} u_s(t) dt$  assuming that  $u_s(t)$  is decreased as in figure 4.9.

In the case of a decrease or increase of the input shaft angular velocity different from the expected, the actuator force will then be corrected. This result in a greater robustness against a too large synchronization force when the slip approaches  $\Omega_{end}$ . Detailed calculations of the integrated forces and calculation of the requested actuator force are presented as commented pseudo-code in appendix B.

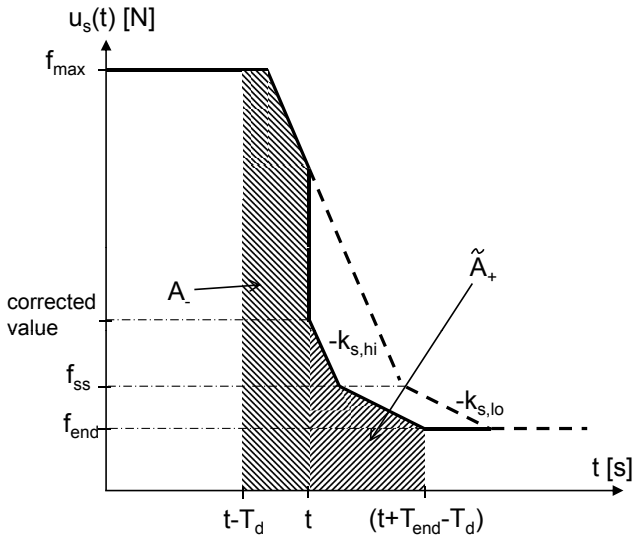


**Figure 4.10.** An example of when the slip decreases faster than predicted. At time  $t$ , the integrated force  $\tilde{A}_+$  is smaller than the integrated area should be if the force request  $u_s(t)$  is kept decreasing with the desired slopes. A calculation of the force that results in the right "area" is made and used as the force request.

## 4.4 Pressure Calculation

This last block handles calculation of the pressure request for the two hydraulic lines. It also handles compensation of the static friction and detent forces as well as the input shaft drag. Table 4.8 shows the input and output signals of the block.

Signal	Type	Description
$u_i(t)$ , $i = s$ or $t$	Input	Requested force from controller block.
<i>BackPressure</i>	Input	Requested idle pressure of the idle hydraulic line.
<i>DetentEstimation</i>	Input	Estimation of the detent force.
<i>StaticFrictionEstimation</i>	Input	Estimation of the static and coulomb friction force.
<i>DragEstimation</i>	Input	Estimation of the input shaft drag.
<i>GearRequest</i>	Input	Requested gear. Used to determine which hydraulic line that is desired to use as active.
<i>State</i>	Input	Used to determine if the input shaft drag compensation should be used ( $State = \pm 2$ ).
$p_{1req}(t)$	Output	Pressure request of line one.
$p_{2req}(t)$	Output	Pressure request of line two.

**Table 4.8.** Table of inputs and outputs in the *Pressure Calculation* block.

After compensation, the final force request is

$$\begin{aligned}
 F_{req}(t) &= \\
 &= u_i(t) - DetentEstimation - StaticFrictionEstimation - DragCompensation
 \end{aligned}
 \tag{4.15}$$

The *DragCompensation* is calculated with the use of equation 2.15

$$\begin{aligned}
 & \text{DragCompensation} = \\
 & = \begin{cases} \min \left( -\frac{\sin(\theta_{cone})}{r_m \mu_{cone} \text{sgn}(\omega_s(t))} \cdot \text{DragEstimation}, u_i(t) \right) & , \text{State} = 2 \\ \max \left( \frac{\sin(\theta_{cone})}{r_m \mu_{cone} \text{sgn}(\omega_s(t))} \cdot \text{DragEstimation}, u_i(t) \right) & , \text{State} = -2 \\ 0 & , \text{else} \end{cases} \quad (4.16)
 \end{aligned}$$

Note here that  $u_i(t)$  is negative during synchronization of the gear in negative direction and that *DragEstimation* always is negative.

The values of *DragCompensation* prevents the total requested force to be less than  $-(\text{DetentEstimation} + \text{StaticFrictionEstimation})$  during synchronization of the gear at positive side and to be greater than

$-(\text{DetentEstimation} + \text{StaticFrictionEstimation})$  during synchronization of the gear at negative side. As a consequence, if the magnitude of the force required to compensate for the drag is greater than the requested force  $u_s(t)$ , but with different sign, fully compensation is not possible (i.e. it is not possible to generate a torque from the synchronizer with the same sign as the slip).

After compensation, the pressure has to be calculated. During synchronization in positive direction, the desired active hydraulic line is number one (and negative number two). The requested idle pressure is set as pressure request at the idle side and thus an additional compensation must then be done at the active side. Equation 2.1 – 2.2 can now be used to calculate the active side pressure request. Equation 4.17 shows how this is done. If the calculation of the active line request gets below zero, the active hydraulic line is switched. Of course it is not desirable to switch active hydraulic line during the synchronization process. The problem is to balance the idle pressure so that no switching occurs, without saturation of the active hydraulic line. Anyway, this switching functionality must exist.

$$\begin{aligned}
 p_{1req}(t) &= \frac{F_{req}(t) + A_2 \text{BackPressure}}{A_1} \quad , \text{when line one is the active line} \\
 p_{2req}(t) &= \frac{-F_{req}(t) + A_1 \text{BackPressure}}{A_2} \quad , \text{when line two is the active line}
 \end{aligned} \quad (4.17)$$



# Chapter 5

## Results

This chapter presents some result of the simulations of the developed software. There are a lot of possible cases to analyze. All model and control parameters – and there is a lot of them – can be varied in different ways. However, the analysis focus lies in a few cases that are found interesting and important in respect to robustness and demonstration of difficulties. The chosen cases are

- Normal conditions
- Negative vs positive slip during cold conditions i.e. large amount of input shaft drag
- Different sample times
- The detent force profile used in the estimation is different from what is used in the simulation plant
- The uncertain model parameters used in the control system differs from those used in the simulation plant
- Sensor noise and backlash
- Use of position prediction

If nothing else is noted in connection to a presented plot, the following values are used:

- A sample time of  $T_s = 3.125$  ms.
- The oil temperature is set to  $60$  °C.
- One friction surface ( $n_r = 1$  in equation 2.15) is used in the synchronizer model in the simulation plant.
- A request of the gear at the positive side occur after 0.1 s and a request of the gear at negative side after 0.7 s. The slip of the positive gear is about 250 rad/s ( $\approx 2500$  rpm) when the synchronization process starts and the slip of the negative gear is about 125 rad/s ( $\approx 1250$  rpm) when the positive gear is engaged.
- P(I)D parameter values of table 4.5 are used with a value of the gain  $K$  in equation 4.10 as  $K = 0.3\tilde{K}$ , except in the engaging interval where a value of  $K = 0.05\tilde{K}$  is used.
- A time of 50 ms from that a state transition occurs until the integration part is added (See explanation of the *CalcControlParams()* function in table C.1).
- The reference signals are changed in one single step in all states except the *Engage* and *Disengage* states ( $\pm 4$  and 10 referred to figure 4.2 or figure C.1 in appendix C), where a ramp slope of  $\pm 0.1$  mm/ms is used.
- The design parameters in the manual synchronization controller are set as
  - $f_0 = 15$  [N]
  - $f_{ss} = 75$  [N]
  - $f_{end} = 35$  [N]
  - $k_{s,lo} = 4 \cdot 10^3$  [N/s]
  - $k_{s,hi} = 2 \cdot 10^4$  [N/s]
  - $\Omega_{end} = 5$  [rad/s]
  - $f_{max} =$  [N]

The state *after synchronization* ( $\pm 3$ ) is used to stable the sleeve at the position  $l_{dogg,start}$  where dogging effects may start. However, simulations shows that the dogging effects implemented in the used simulation plant does not affect the synchronization process at all. The states ( $\pm 3$ ) are however still used, if nothing else is noted. It has been shown that the brake of the sleeve at this point decreases the undesired acceleration caused by the detent force. That is why the state still is used. However, in the case of a large synchronization force in the end of the synchronization, the sleeve will still pass this position with a large velocity and a transition to state *engage* ( $\pm 4$ ) occurs without any try to stabilize the sleeve at the dogging start position  $l_{dogg,start}$ .

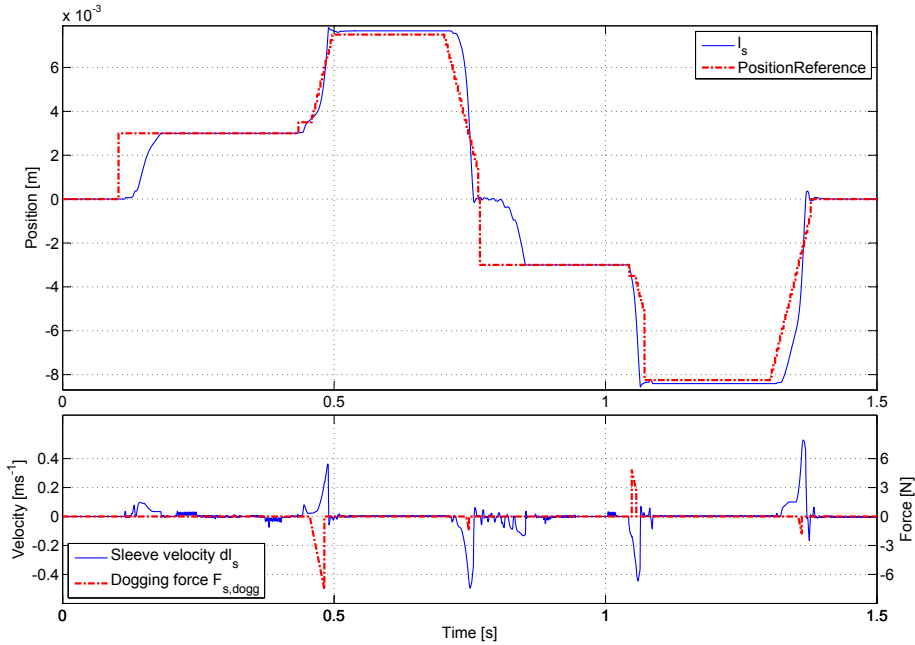


**Figure 5.1.** The upper plot shows the position reference and sleeve position during a simulation of normal conditions. The synchronization occurs at  $l_s = \pm 3$  mm and the detent force starts to increase/decrease at position  $l_s \approx 3.5 / -3.5$  mm. The lower plot shows the sleeve velocity (left y-axis) and dogging force (right y-axis). The speed of the sleeve is less than 0.1 m/s when it hits the synchronization position and about 0.4 m/s when it hits the end stop. The dogging force occurs in the interval  $3.5 \text{ mm} \leq |l_s| \leq 5 \text{ mm}$  but does not seem to affect the sleeve movement at all. The engagement of the gear at the positive side takes about 400 ms and the engagement of the gear at the negative side takes about 300 ms.

## 5.1 Normal Conditions

Figure 5.1 shows the sleeve position and the position reference signal in the upper plot. Because of the system delay and the fast increase of the detent force around neutral position, the detent estimation error is large and the sleeve velocity is small close to neutral position. The saddle point in the sleeve position at about  $l_s = 3.5$  mm is where the detent force starts to increase from its minimum value. That is why the sleeve is accelerated the last interval towards the end stop. The detent force can be reviewed in figure 2.8 or 5.7.

In the lower plot of figure 5.1, one can see the sleeve velocity and the dogging forces. No reasonable values for the velocity at the synchronization and end stop positions are known, but they can be compared to the values of simulations of other conditions presented later in this chapter. The dogging forces do not affect the synchronization process at all.

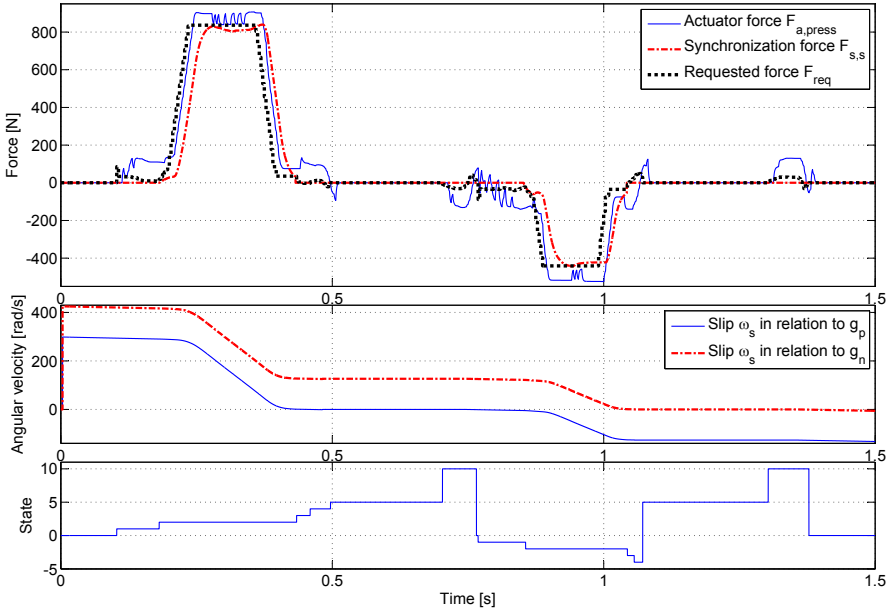


**Figure 5.2.** The upper plot shows that the synchronization force follows the desired behaviour presented in figure 4.9. The oscillations of the actuator force at time  $t = 0.7 - 0.8$  s occur because of the disengagement. Note that the actuator force  $F_{a,press}$  sometimes is significantly larger than zero at the same time as the controller output  $u_i$  is almost zero. This is due to compensation of the static friction and detent forces. The middle plot shows the slip related to gear  $g_p$  and  $g_n$  and the lower plot shows the state of the state machine.

Figure 5.2 shows the actuator force  $F_{a,press}$ , the synchronization force  $F_{s,s}$  and the requested force  $u_i$  from the controller block. Note that because of compensations, the actuator force differs from the controller force. The oscillations in the actuator force when it reaches its largest magnitudes is because of the static and coulomb friction compensation. This compensation should maybe be turned off during usage of large actuator forces. The synchronization force follows the desired behaviour shown in figure 4.9 in chapter 4.3.2. The middle plot of figure 5.2 shows the slip related to the gears at the positive and negative sides. The first synchronization takes 240 ms and eliminates a slip of 290 rad/s which is 1210 rad/s<sup>2</sup>. The second synchronization takes 150 ms and eliminates a slip of 125 rad/s and that is 830 rad/s<sup>2</sup>. The reason of the slower synchronization in the second case is that the actuator area  $A_2$ , which is the one at the active hydraulic line during synchronization of the gear at the negative side, is smaller than the area  $A_1$ . This enables smaller actuator force in negative direction. The lower plot of figure 5.2 shows the state of the state machine. It can for example be used to detect for how long the sleeve is in synchronization position ( $State = \pm 2$ ).

To illustrate the problems with large sleeve acceleration during the engage interval, figure 5.3 shows a zoom of that interval and the disengage interval. The detent force is increasing for sleeve positions greater than  $3.5\text{ mm}$ . The dash-dotted signal shows the fork position measurement ( $y_1$ ) delayed with the time  $T_{ad} + T_{cd}$ . This is the feedback signal to the controller when it is calculating the pressures that affects the fork. This delay problem is worsen by the fact that there is a detent compensation. Compare this to a case where you have a delay between your eyes and your brain while your are pushing something over a hill top. When the thing you are pushing is right after the top of the hill, on its way down, you are pushing a little bit extra because you think it has not reached the top.

The simulation shows that the detent force behaviour between synchronizaton and end stop positions combined with the system delay may be a problem in case of a desired smooth end stop enclosure.

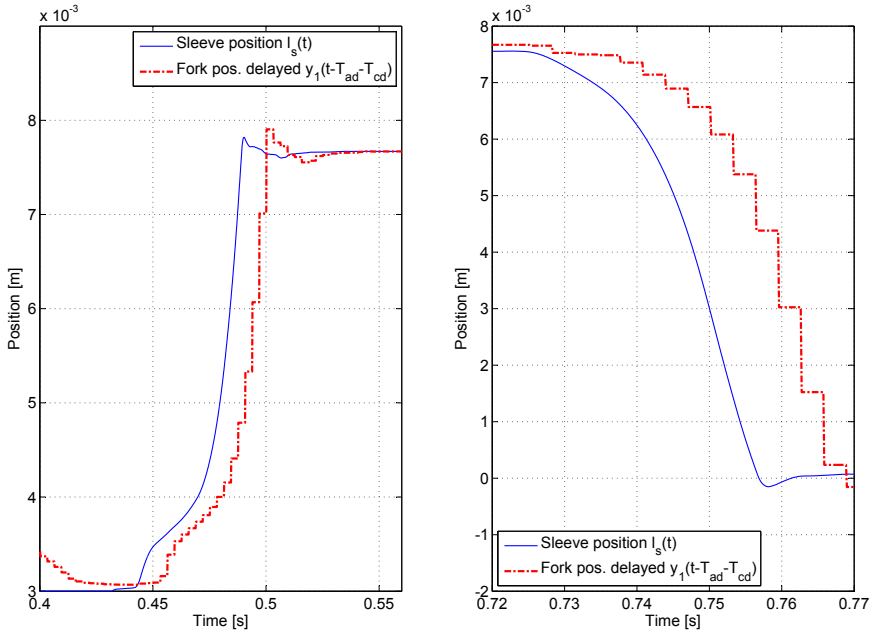


**Figure 5.3.** The left plot shows the sleeve position of the after synchronization and engage intervals during engagement of gear  $g_p$ . Problems in controlling the movement in a smooth way can be explained by the delay  $T_{ad} + T_{cd}$  that affects the system. The position measurement  $y_1$  is displayed as  $y_1(t - T_{ad} - T_{cd})$  to illustrate the delay effects. A look at the delayed signal of time  $t = 0.48$  s gives the position  $\approx 4$  mm. This is what is used in the controller and detent estimation when the force that propagates on the fork at this time is calculated. When the calculated force "reaches" the actuator fork, the fork and the sleeve positions are about  $l_f \approx l_s \approx 5.5$  mm. The right plot shows the disengage interval. The detent force is positive (counteracting) when the sleeve position is between 4.5 and 7.5 mm. For positions between zero and 4.5 mm it is negative (helping). The fast brake of the sleeve at neutral is rather because of the detent force than of the controlled pressures.

## 5.2 Cold Conditions

Two simulations using an oil temperature of  $10\text{ }^{\circ}\text{C}$  are made, which gives rise of a larger amount of input shaft drag. The gear request of the positive gear here comes at time zero. The first simulation shows a slip of  $+30\text{ rad/s}$  and in the second simulation the slip is  $-30\text{ rad/s}$ . Figure 5.4 shows the sleeve position and the slip of the gear at the positive side. In the case with positive slip, the drag helps the synchronization. Compensation is made and if the drag helps the synchronization, the requested force is decreased. But as was mentioned in chapter 4.4, fully compensation is not always possible in that case.

In the case of negative slip, the magnitude of it increases in the beginning. The sleeve is released from synchronization position while a large amount of actuator force is applied. This is due to the drag compensation which must be used to eliminate the slip. The position reference is ramped with  $0.1\text{ mm/ms}$  in the engage state and therefore the sleeve turns back. In this case it passes the synchronization position again. As can be seen in the lower plot, the magnitude of the slip has increased again when the sleeve moves back. In reality, a new synchronization should have to be performed and the scenario would then be repeated and the gear not engaged (because of the simulation plant, no synchronization force occur if the magnitude of the slip is lower than  $20\text{ rad/s}$  when the sleeve hits the synchronization position).

Figure 5.5 shows the synchronization force and the requested pressure of line one during the simulation. As can be expected, the synchronization force is much greater in the case of negative slip. In both cases, the synchronization force in the end of synchronization is larger than desired.

Because of that fully drag compensation is not possible during the final synchronization in the positive slip case, the error in the input shaft angular velocity prediction made in the algorithm of the manual controller gets large (i.e. the algorithm calculates an integrated force that should be used to eliminate the slip but this "area" is too large because the drag is not included). That is why the synchronization force is too large during the final synchronization. Anyway, it is not that large that the sleeve accelerates toward the end stop as in the case of negative slip. A large synchronization force is in that case impossible to avoid because of the need of drag compensation.

The problem of the sleeve turning back can easily be solved by a transition directly from the state synchronization to engage, combined with a large slope of the position reference. However, the problem with a large sleeve velocity when it hits the end stop remains. The problems of a large error in the angular velocity prediction during positive slip and large drag can be solved by including the drag estimation in the integration in equation 4.11. Another and easier approach is to increase the design parameter  $\Omega_{end}$  used in the manual controller, which will decrease the synchronization force earlier.

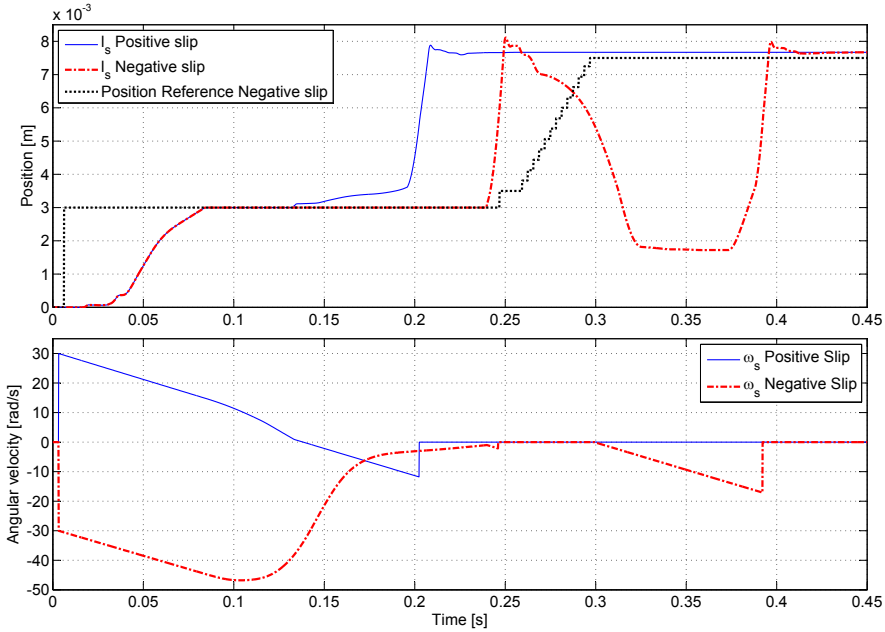


**Figure 5.4.** The upper plot shows the sleeve positions from the simulations of cold conditions. It also contains the position reference of the simulation of negative slip. The lower plot shows the slip of the gear of at the positive side in the two simulations. In the case of negative slip, the sleeve leaves the synchronization position with a large acceleration and hits the end stop with a very large velocity while the position reference remains at 3.5 mm. Because of that, it is moved back to almost neutral position. The magnitude of the slip increases in the beginning of the negative slip case. That is because the applied force has not "reached" the synchronization friction rings yet. The instantaneous elimination of the slip at about  $t = 0.2$  and  $t = 0.4$  is because of the simulation plant, since when the sleeve reaches the engaged position beyond the dogging position, the input shaft angular velocity is set as  $-i\omega_o$ .

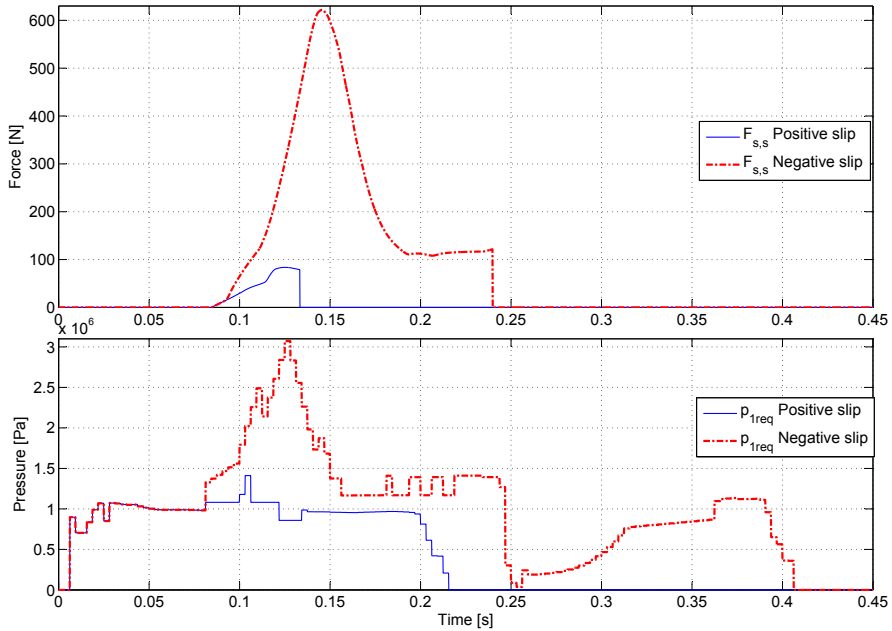


**Figure 5.5.** The upper plot shows the synchronization force of the two simulations and the lower plot shows the pressure requests of line one. The large amount of synchronization force at the end of the synchronization in the negative case causes a large acceleration of the sleeve. The pressure request during positive slip simulation shows no ramp increase like during negative slip. The reason for this is that compensation of the "helping" drag is made.

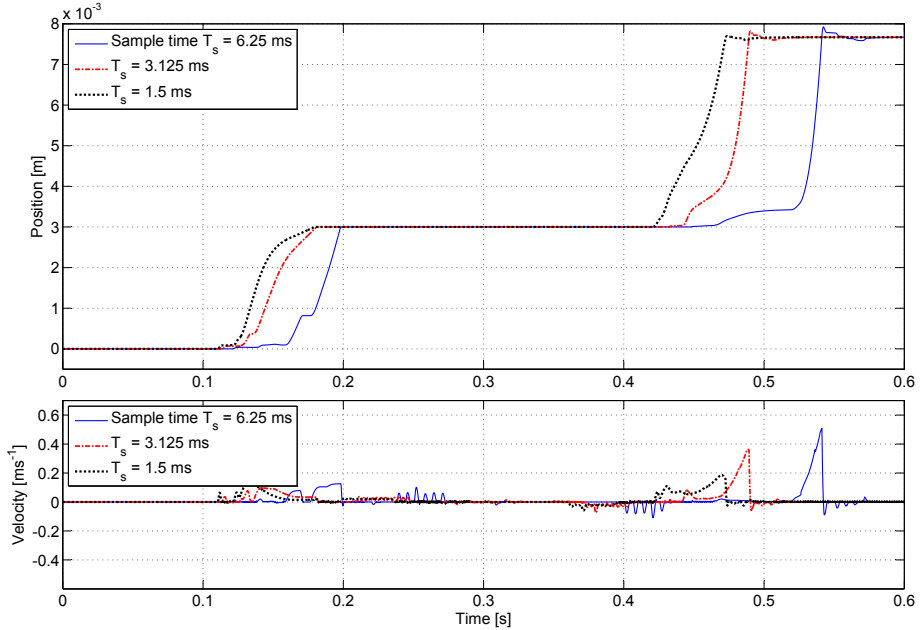


**Figure 5.6.** A plot of sleeve position and velocity during three simulations under normal conditions using different sample times. The PID parameters are recalculated in each simulation using equation 4.9 and table 4.5.

### 5.3 Different Sample Times

Figure 5.6 shows the sleeve position when the normal sample time is used. It also contains the sleeve position of simulations where the double and half the sample time are used. The lower plot shows the sleeve velocity in the same simulations. As expected, a lower sample time result in a more controlled movement with less velocity fluctuations. The system delay is also lower with a lower sample time because the assumption that the control delay is equal to the sample time. The different times it takes to eliminate the slip is harder to explain. A lower sample time updates the increase and decrease of the requested force in the manual synchronization controller more often. This may cause different synchronization forces. Remember that there are lots of dynamics between the requested pressure and the synchronization force. This should then also explain the larger amount of synchronization force in the end of the interval when the smaller sample time is used. As can be seen, the sleeve does not stop at the dogging position in the half sample time case. But it has anyway a lower velocity when it hits the end stop.

If another sample time is used, the control parameters, especially those of the manual controller, should be tuned.

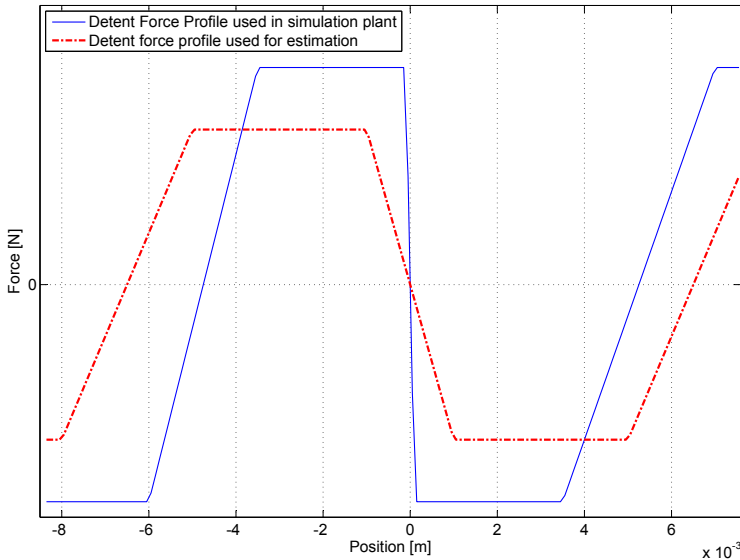


**Figure 5.7.** The detent force used in the simulation plant vs the one used for compensation. There are both magnitude and behaviour differences.

## 5.4 Different Detent Compensations

It is not probable that an exact knowledge of the detent force can be obtained. Therefore, one simulation is made where no detent force compensation is used. A second simulation is performed, where a detent force profile different from the one used in the simulation plant, is used for estimation and compensation. This difference is displayed in figure 5.7. Figure 5.8 shows the sleeve positions and velocities of the two simulations. Because of the errors in the compensation, the sleeve is stuck close to the neutral position until the integration part in the PID controller is added. At the end of synchronization, the applied force is less than the detent force if  $f_{end}$  is not large enough, and the sleeve is pushed back towards neutral by the detent force. The design parameters  $f_{end}$  and  $f_{ss}$  are set to 100 and 150 [N] respectively in this simulation to prevent those effects. One can also see that the velocities are larger when the sleeve hits the synchronization and end stop positions compared to the normal case in section 5.1, which is explained by the integration part in the controller and the detent estimation error.

An integration part of the transportation controller and a larger value of  $f_{end}$  and  $f_{ss}$  is needed in case of no or wrong detent compensation. A compensation different from the real detent force should lead to less control of the sleeve movement when it hits the synchronization and end stop positions.

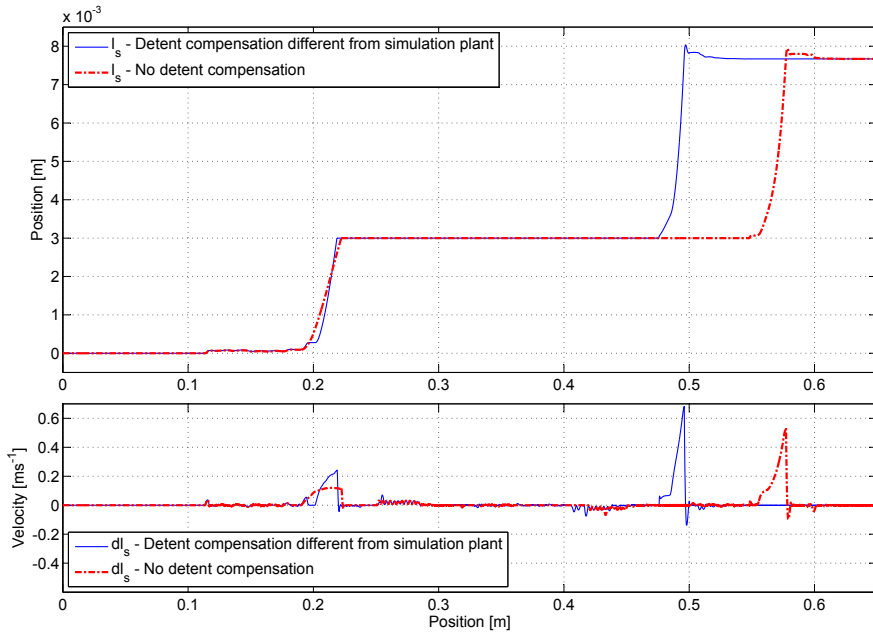


**Figure 5.8.** Sleeve position and velocity during simulations with different detent force profiles used in the estimation. There is a difference in the synchronization time of about 80 ms between the two cases. This is because the error between the detent force and its estimation is "stolen" from the synchronization force.

## 5.5 Parameter Variations and Sensor Backlash

A final test is performed where the parameters in the simulation plant are changed while those used in the control software are unchanged. The parameter variation is made by generating random numbers between 0.5 and 1.5. Then the parameters are multiplied with these numbers and for every one, a new number is generated. The parameters and their corresponding random factor are listed in table 5.1. Three simulations are made and figure 5.9 shows the sleeve positions and velocities. A backlash of 0.2 mm in the position sensor is also simulated here. Figure 5.10 shows the slip related to the gears  $g_p$  and  $g_n$ . In the lower plot the synchronization forces are shown.

The tests are performed several times and shows almost the same result. The difference in synchronization time can be explained by the differences of the cone friction  $\mu_{cone}$  which generates the synchronization torque. In the second simulation, the cone friction  $\mu_{cone}$  is very low and the synchronization is finished right before the gear request is changed. The velocities at the end stop position in simulation one and three are not significantly larger than in the normal case. But the velocities when the sleeve hits the synchronization point are about the double of the normal case. The sleeve is also stuck close to neutral position until the integration part in the PID controller is added (after 50 ms). This and the larger velocities can possibly be explained by the sensor backlash which raises a larger detent force estimation error at positions where the detent force changes fast. The difference in spring and damping effects may worsen the detent estimation error even more. Because of the softer spring effects, that results in larger difference between fork and sleeve positions. The fork position is used to estimate the detent force which in real case is dependent on sleeve position.

The dynamic and viscous frictions are greater in the second simulation and a look at the velocity shows the damping effects this has. In the first simulation, the frictions are smaller and this case shows the highest velocities of the three simulations. The variations in static frictions show no problems. In this case the variations are too small to affect the performance. In case of larger static frictions, it is important to calibrate a value to enable compensation. Otherwise the static friction will "steal" force that is meant to be used to accelerate the sleeve or synchronize the shafts.

The hydraulic valve dynamics are too small to affect the performance. The value of  $a_h$  is less than the sample time and shows no influence on the synchronization process at all. The influence of the actuator delay has already been explained to be significant. A large difference between estimated and real delay raises a large error in the angular velocity prediction in the manual controller.

In case of uncertainty in the knowledge of the friction  $\mu_{cone}$ , a lower ramp slope  $k_{s,hi}$  used in the manual controller may help. The parameters of the controllers should be tuned in respect of the system frictions. The more damped the sleeve movement is, the larger controller gains and forces can be used.

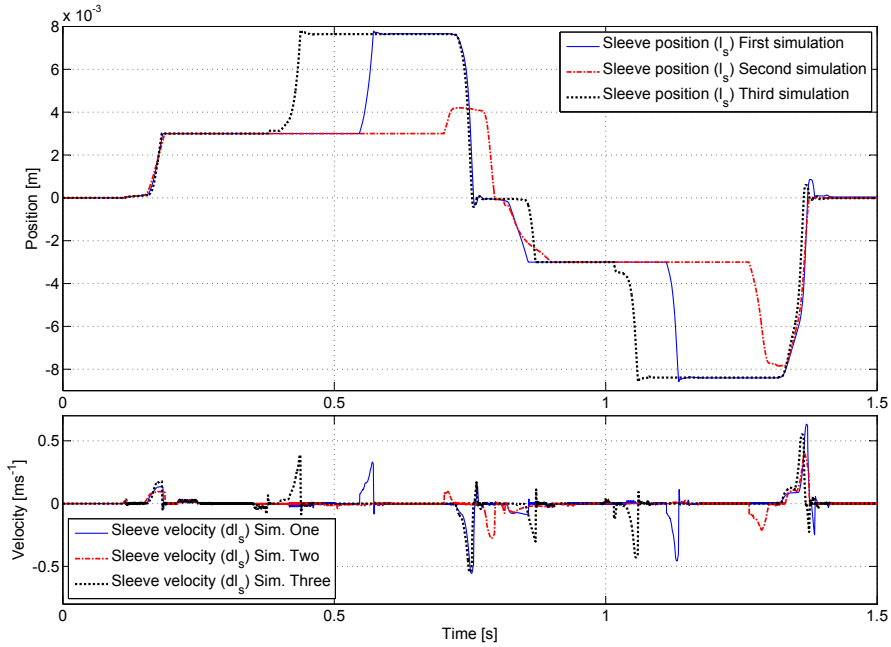


**Figure 5.9.** Sleeve position and velocity of three simulations where the parameters in table 5.1 are varied. In the second simulation, the synchronizations of both gear  $g_p$  and  $g_n$  are finished right before a new gear request occurs and the gear are not engaged. This is because of a very low friction coefficient  $\mu_{cone}$ .

Parameter	Generated factor in Sim. one	Generated factor in Sim. two	Generated factor in Sim. three
$T_{ad}$	99%	63%	115%
$a_h$	99%	144%	123%
$\mu_{a,vf}$	84%	146%	115%
$f_{a,coulomb}$	140%	108%	95%
$f_{a,static}$	87%	56%	105%
$k_{fs}$	61%	73%	80%
$c_{fs}$	128%	85%	124%
$\mu_{s,df}$	89%	132%	69%
$\mu_{cone}$	74%	52%	119%

**Table 5.1.** List of generated factors of the simulations using different simulation plant parameters.

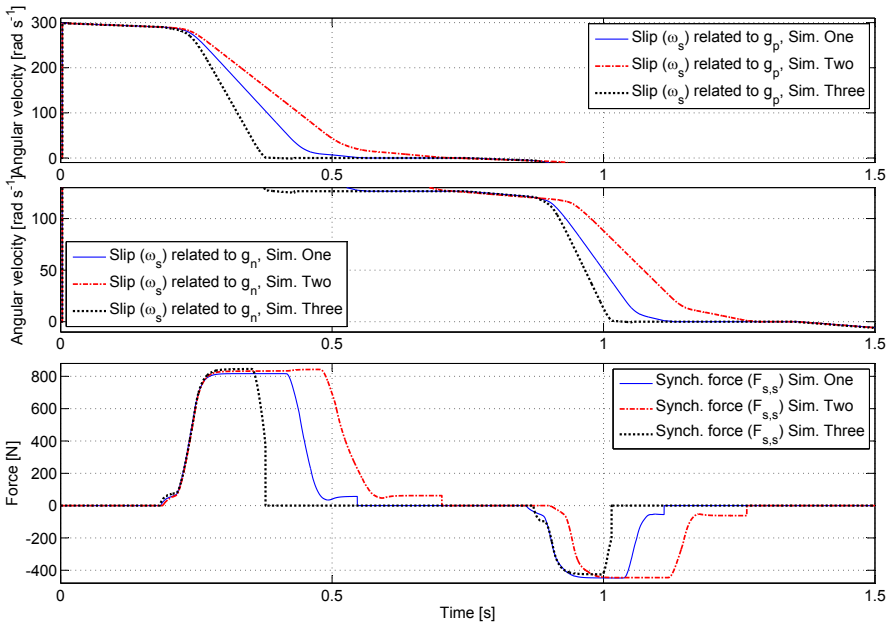
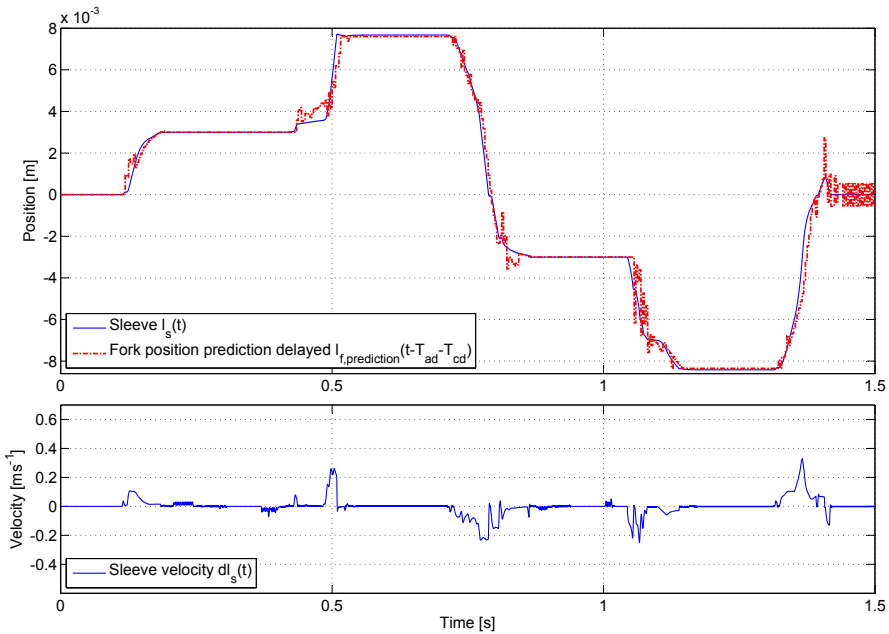


**Figure 5.10.** Slip and synchronization force of the three parameter variation simulations. Note that the gears are synchronized (the slip is zero) also in the second simulation. The magnitude of the synchronization force is equal in the beginning of the three simulations. Hence, the ratio of the slip decrease can be related to the value of the cone friction  $\mu_{cone}$ .

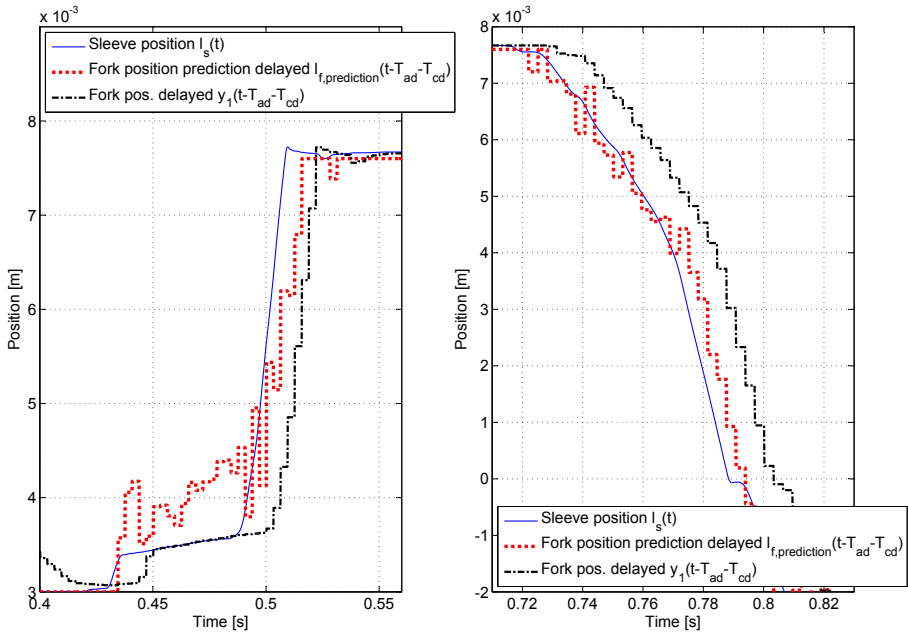
## 5.6 Fork Position Prediction

Figure 5.11 shows the sleeve position and velocity during a simulation of normal conditions described in chapter 5.1. The difference compared to chapter 5.1 is that the fork position prediction, presented in chapter 4.2.1, is used as input to the detent estimation. The prediction, delayed by the time  $T_{ad} + T_{cd}$  is also showed in the upper plot of figure 5.11. There is an oscillative behovaieur in some intervals and that is the reason it is not used as feedback to the PID controller. A comparison between the velocity plot in figure 5.1 and figure 5.11 shows that the sleeve velocity is lower at the end stop positions when the prediction is used as detent estimation input. Moreover, the velocity is close to zero when it hits the synchronization point. Figure 5.12 shows the same zoom in of the after synchronization, engage and disengage intervals as in figure 5.3. Here one can see how much less the position error is when the prediction is used. The plots in figure 5.12 also shows the delayed fork position that was used as the input to detent estimation in the first normal conditions simulation. However, further development of the prediction is needed if it is going to be used as controller feedback. For example, the prediction right after the synchronization is not good.

Usage of the prediction algorithm demands knowledge about the system parameters like for example static and dynamic friction forces and actuator delay.



**Figure 5.11.** Sleeve position and velocity during normal conditions, with position prediction used as detent estimation input. The upper plot also shows the prediction, delayed with the forward predicted time  $T_{ad} + T_{cd}$ . The oscillative behaviour in some intervals makes it unsuitable to be used as controller feedback. However, the velocity is close to zero when the sleeve hits the synchronization positions and when it hits the end stop of the negative side. It is also decreased to about 0.25 m/s compared to  $\approx 0.4$  m/s when it hits the end stop at the positive side.



**Figure 5.12.** A zoom of the sleeve position at the after synchronization, engage and disengage intervals at the positive side (same type as figure 5.3) The prediction shows a larger error in the after synchronization interval, but a smaller error of the other intervals, compared to the case when the fork position measurement is used as input to the detent estimation.

# Chapter 6

## Discussion

The simulation results show that the synchronization process takes 200 – 500 ms during the studied conditions. The simulations in chapter 5.5 also shows that there is a robustness in the chosen control design. In cases of a not that good control, some software corrections are suggested in connection to those results.

Almost every model parameter affects the performance in some way. Values like mass, moment of inertia, radius, gear ratio and actuator piston areas can be measured with high precision and should not show any substantially changes during a gearbox lifetime. Other model parameters which are more important to calibrate are the detent force, system delay, input shaft drag and friction affecting the actuator system and synchronizer sleeve.

As shown in the simulation of different detent force profiles used in the estimation, the detent force has a big impact on how accurately the sleeve movement can be controlled. A calibration of the positions where the detent force goes from constant to increasing or decreasing may be done by applying a constant actuator force. The position of where the large acceleration starts should then be close to this position. The minimum and maximum detent forces, assuming that they are constant in some interval, can also be calibrated. For example the minimum force applied when the sleeve is in synchronization position, and still not "falls" back to neutral, should be the magnitude of the detent force at this position. One problem is that static friction forces are impossible to separate from the detent force in such tests. The same can be done when the sleeve is forced against the end stop. These tests should be made with the presumption of a detent force profile close to that in figure 2.8.

The delay is important to know when controlling a system. Delays have generally a significant impact on a controlled system, and especially it affects the result of the manual synchronization algorithm in this work. An error in the prediction of the input shaft angular velocity may result in that the sleeve is stuck in the synchronization position too long (like in the second simulation of varying parameters in chapter 5.5). It can also result in a large acceleration of the sleeve after synchronization. There are no difficulties to measure a delay like this, as long as it remains constant. However, information from [10] indicates that different delays

and dynamics occur in the hydraulic valves during different pressures. This extensively obstructs the control of the synchronization process. In worst case, the control needs to be split up in several intervals, dependent on the pressure.

The input shaft drag affects the time of synchronization. It also affects the synchronization force during the final synchronization as shown in the simulations of cold conditions in chapter 5.2. The method of drag estimation presented in chapter 4.2.3, leaves possibilities to include the drag in a transfer function of the synchronization interval or in the manual synchronization algorithm. However, several transfer functions should be used dependent on the temperature. As a suggestion, one for normal and one for cold conditions. If the drag estimation model is included in the manual controller, it perplexes the integration in equation 4.11.

Friction acting on the fork and sleeve and in the hydraulic system may be hard to measure. In simulation one of the parameter variations (chapter 5.5), both the dynamic and viscous frictions are low, while they are larger in simulation two. The sleeve velocity in the two cases shows the damping effects a larger friction force result in. If the friction is larger than the values used in these simulations, the acceleration effects of the detent force may not be a problem.

It is important to point out that the seven parameters of the manual synchronization controller are meant to be design parameters. There are a lot of approximations made in the development and the parameters should be tuned to get the synchronization performed in a desired manner.

The simulation where position prediction is used in detent estimation shows a little of the advantages with predicting the position. A prediction stable enough to be used as feedback in the PID controller will probably show a great improvement of smooth control. More work should be dedicated to either a sophistication of the existing prediction or some other method.

Assuming the modeling results of this thesis are accurate, the result shows that it is possible to engage a gear in a few tenths of a second with the use of an actuator system like the one treated here. However, particularly the impact of dogging forces and sensor noise should be verified in detail on a real system.

# Chapter 7

## Future Work

An investigation of the drag should be performed and maybe the model needs to be changed. It can be calibrated using equation 2.17. However, measurements or estimations of the oil temperature is needed both for calibration and control.

The most important investigation that remains, is maybe the impacts of the dogging forces. In these simulations they do not affect the performance at all. However, as earlier been mentioned, the dogging force may be much larger in some cases. The fact that it occurs at a random position could significantly obstruct the control.

Some extra functionalities should be added in the control software to handle problems during special conditions, i.e. negative/positive slip, small/large slip, cold conditions etc. Some suggestions to solve such problems were stated in connection to the simulation results in chapter 5. A large number of simulations under different conditions should be performed to find out other important special conditions.

The developed transfer function may be used to implement an observer using kalman filter technique [4] and linear quadratic control design [4]. However, one problem is the discontinuous behaviour in the transition between transportation and synchronization and vice versa. Also the nonlinear forces acting on the sleeve obstructs the usage of an observer.

An attempt to use internal model control (IMC) [4], which is a method sometimes used to solve problems with delays, may show improved results.

The way of holding one pressure constant and treating the control signal as one force request works fine in this thesis. However, active control of both pressures may improve the performance.



# Chapter 8

## Variable and Parameter Lists

There are a large number of variables and parameters used in this report. Most of them are listed with a short description in the tables below. The rest are only mentioned in a single paragraph and explained in connection to that.

Variable	Description	Unit
$l_f$	Actuator fork position	$m$
$l_s$	Synchronizer sleeve position	$m$
$\omega_i$	Input shaft angular velocity.	$rad \cdot s^{-1}$
$\omega_o$	Output shaft angular velocity.	$rad \cdot s^{-1}$
$\omega_s$	Slip between input and output shaft. $\omega_s = \omega_i - i\omega_o$ , where $i$ is the actual gear ratio.	$rad \cdot s^{-1}$
$p_1, p_2$	Pressure in the actuator system pressure line one and two.	$Pa$
$p_{1req}, p_{2req}$	Requested pressure in the actuator system pressure line one and two (system input signals).	$Pa$
$F_{a,press}$	The resultant force from the hydraulic system propagating on the actuator fork.	$N$
$F_{a,sc}$	Friction force generated by static or coulomb friction in the actuator system.	$N$
$F_{a,vf}$	Friction force generated by viscous effects in the hydraulic system.	$N$
$F_{fs}$	Spring and damper forces in the attachment between the actuator fork and synchronizer sleeve.	$N$
$F_{s,df}$	Dynamic friction force acting on the synchronizer sleeve.	$N$
$F_{s,s}$	Synchronization force (normal force between synchronizer sleeve and the friction rings).	$N$
$F_{s,det}$	Detent force propagating on the synchronizer sleeve.	$N$
$F_{s,dogg}$	Dogging force generated by dogging effects between the sleeve and the gear wheel.	$N$
$M_a$	Synchronization torque applied at the input shaft.	$N \cdot m$
$M_{drag}$	Drag torque due to losses acting on the input shaft.	$N \cdot m$
$k_{drag}$	Estimated oil temperature dependent variable used to approximate the input shaft drag.	$N \cdot m \cdot s$
$m_{drag}$	Estimated oil temperature dependent variable used to approximate the input shaft drag.	$N \cdot m$
$\tau$	Gear box oil temperature.	$^{\circ}C$
$y_1$	System output one, actuator fork position.	$m$
$y_2$	System output two, input shaft angular velocity.	$rad \cdot s^{-1}$
$y_3$	System output three, output shaft angular velocity.	$rad \cdot s^{-1}$

**Table 8.1.** List of variables.

Parameter	Description	Unit
$g_p, g_n$	Gear number in positive and negative direction at the gear gate.	1
$i_p, i_n$	The gear ratios of gear $g_p$ and $g_n$ above.	1
$T_{ad}, T_{cd}$	Actuator delay and control delay.	s
$T_s$	Sample time.	s
$l_{neutral}$	Synchronizer sleeve neutral position.	m
$l_{synch}$	The synchronization position of the sleeve.	m
$l_{dogg,start},$ $l_{dogg,end}$	Start and end of dogging effects in worst case (i.e. when the sleeve position is between these points, both negative and positive, dogging effects can occur).	m
$A_1, A_2$	Actuator fork areas in contact with the hydraulic oil in pressure line one and two.	$m^2$
$m_f, m_s$	Mass of the actuator fork and synchronizer sleeve.	kg
$\mu_{a,vf}$	Friction coefficient of viscous friction in hydraulic system.	$kg \cdot s^{-1}$
$\mu_{s,df}$	Friction coefficient of dynamic friction acting on the sleeve.	$kg \cdot s^{-1}$
$\mu_{cone}$	Friction coefficient of friction surfaces at the intermediate ring in the synchronizer.	1
$k_{fs}$	Spring rate of the spring and damping effects between the fork and the sleeve.	$N \cdot m^{-1}$
$c_{fs}$	Damping rate of the spring and damping effects between the fork and the sleeve.	$N \cdot s \cdot m^{-1}$
$a_h$	Time constant of the hydraulic pressure valves.	s
$\theta_{cone}$	Angle of the friction cones in the synchronizer.	rad
$r_m$	Mean radius of the friction rings.	m
$J_i$	Moment of inertia of the input shaft.	$kg \cdot m^2$
$L_b$	Backlash in the fork-sleeve attachment.	m

**Table 8.2.** List of parameters.



# Bibliography

- [1] Karl Gustav Andersson. *Lineär algebra*. Studentlitteratur, 2 edition, 2000. ISBN 91-44-01608-5.
- [2] Marshall Brain. How manual transmissions work, 2000. <http://auto.howstuffworks.com/transmission.htm>.
- [3] Linköping University Department of Automatic Control. Industriell regler teknik.
- [4] Torkel Glad and Lennart Ljung. *Reglerteori, Flervariabla och olinjära metoder*. Studentlitteratur, 2 edition, 2003. ISBN 978-91-44-03003-6.
- [5] William Harris. How dual-clutch transmissions work, 2006. <http://auto.howstuffworks.com/transmission.htm>.
- [6] Mikael Johansson. GMPT employee, 2008.
- [7] Mikael Molin. GMPT employee, 2008.
- [8] Syed T Razzacki (DaimlerChrysler, Inc.). Synchronizer design: A mathematical and dimensional treatise. Technical Report 2004-01-1230, SAE Technical paper series, 2004. Reprinted From: Transmission and Driveline Symposium 2004 (SP-1817).
- [9] Richard J Socin (Chrysler Corp.), L Kirk Walters (General Motors Corp.). Manual transmission synchronizers. Technical Report 680008, SAE Technical paper series, 1968.
- [10] Ole Jonny Waerp. GMPT consultant, 2008.



# Appendix A

## Transfer Function Calculation

This appendix presents the calculations in chapter 3. The physical model equations in chapter 2 are used with a change to the frequency domain (laplace transform representation). Initial values are assumed to be zero.

### A.1 Equation 3.2

The equations 2.1, 2.2 and 3.1 together result in

$$\begin{aligned}\mathbf{F}_{req} &= A_1 \mathbf{P}_{1req} - A_2 \mathbf{P}_{2req} = \\ &= A_1 (a_h \mathbf{s} \mathbf{P}_1 + \mathbf{P}_1) e^{T_{ad} \mathbf{s}} - A_2 (a_h \mathbf{s} \mathbf{P}_2 + \mathbf{P}_2) e^{T_{ad} \mathbf{s}} = \\ &= (a_h \mathbf{s} + 1) (A_1 \mathbf{P}_1 - A_2 \mathbf{P}_2) e^{T_{ad} \mathbf{s}} = \\ &= (a_h \mathbf{s} + 1) (\mathbf{F}_{a,press}) e^{T_{ad} \mathbf{s}} \quad (\text{A.1})\end{aligned}$$

### A.2 Equation 3.3

Combining equations 2.4 – 2.6 result in

$$\begin{aligned}m_f \mathbf{s}^2 \mathbf{L}_f &= \mathbf{F}_{a,press} + \mathbf{F}_{a,vf} + \mathbf{F}_{a,sc} - \mathbf{F}_{fs} = \\ &= \mathbf{F}_{a,press} - \mu_{a,vf} \mathbf{s} \mathbf{L}_f + \mathbf{F}_{a,sc} - (c_{fs} \mathbf{s} + k_{fs}) (\mathbf{L}_f - \mathbf{L}_s) \iff \\ \iff (m_f \mathbf{s}^2 + (\mu_{a,vf} + c_{fs}) \mathbf{s} + k_{fs}) \mathbf{L}_f &= \mathbf{F}_{a,press} + (c_{fs} \mathbf{s} + k_{fs}) \mathbf{L}_s + \mathbf{F}_{a,sc} \quad (\text{A.2})\end{aligned}$$

### A.3 Equation 3.4

Combining equations 2.5, 2.8, 2.9 and 2.13 with the assumption that  $l_s(t) \neq l_{synch}$  or that  $\omega_s(t) \neq 0$  results in

$$\begin{aligned}
 m_s \mathbf{s}^2 \mathbf{L}_s &= \mathbf{F}_{f_s} + \mathbf{F}_{s,df} + \mathbf{F}_{s,det} + \mathbf{F}_{s,dogg} = \\
 &= (c_{f_s} \mathbf{s} + k_{f_s}) (\mathbf{L}_f - \mathbf{L}_s) - \mu_{s,df} \mathbf{s} \mathbf{L}_s + \mathbf{F}_{s,det} + \mathbf{F}_{s,dogg} \iff \\
 \iff (m_s \mathbf{s}^2 + (c_{f_s} + \mu_{s,df}) \mathbf{s} + k_{f_s}) \mathbf{L}_s &= (c_{f_s} \mathbf{s} + k_{f_s}) \mathbf{L}_f + \mathbf{F}_{s,det} + \mathbf{F}_{s,dogg} \quad (\text{A.3})
 \end{aligned}$$

### A.4 Equation 3.5 and 3.6

Equation A.1 and A.3 used in equation A.2 result in

$$\begin{aligned}
 (m_f \mathbf{s}^2 + (\mu_{a,vf} + c_{f_s}) \mathbf{s} + k_{f_s}) \mathbf{L}_f &= \\
 \frac{1}{a_h \mathbf{s} + 1} \mathbf{F}_{req} e^{-T_{ad} \mathbf{s}} + (c_{f_s} \mathbf{s} + k_{f_s}) \frac{(c_{f_s} \mathbf{s} + k_{f_s}) \mathbf{L}_f + \mathbf{F}_{s,det} + \mathbf{F}_{s,dogg}}{m_s \mathbf{s}^2 + (c_{f_s} + \mu_{s,df}) \mathbf{s} + k_{f_s}} + \mathbf{F}_{a,sc} \\
 \iff \left\{ \underbrace{m_f \mathbf{s}^2 + (\mu_{a,vf} + c_{f_s}) \mathbf{s} + k_{f_s}}_{\alpha} - \frac{\overbrace{(c_{f_s} \mathbf{s} + k_{f_s})^2}^{\gamma^2}}{\underbrace{m_s \mathbf{s}^2 + (c_{f_s} + \mu_{s,df}) \mathbf{s} + k_{f_s}}_{\beta}} \right\} \mathbf{L}_f &= \\
 = \frac{1}{a_h \mathbf{s} + 1} \mathbf{F}_{req} e^{-T_{ad} \mathbf{s}} + \frac{\overbrace{c_{f_s} \mathbf{s} + k_{f_s}}^{\gamma}}{\underbrace{m_s \mathbf{s}^2 + (c_{f_s} + \mu_{s,df}) \mathbf{s} + k_{f_s}}_{\beta}} (\mathbf{F}_{s,det} + \mathbf{F}_{s,dogg}) + \mathbf{F}_{a,sc} \\
 \iff \frac{\alpha \beta - \gamma^2}{\beta} \mathbf{L}_f = \frac{1}{a_h \mathbf{s} + 1} \mathbf{F}_{req} e^{-T_{ad} \mathbf{s}} + \frac{\gamma}{\beta} (\mathbf{F}_{s,det} + \mathbf{F}_{s,dogg}) + \mathbf{F}_{a,sc} \iff \\
 \iff \mathbf{L}_f = \underbrace{\frac{\beta}{(\alpha \beta - \gamma^2) (a_h \mathbf{s} + 1)} e^{-T_{ad} \mathbf{s}} \mathbf{F}_{req}}_{G_t} + \underbrace{\frac{\gamma (\mathbf{F}_{s,det} + \mathbf{F}_{s,dogg}) + \beta \mathbf{F}_{a,sc}}{\alpha \beta - \gamma^2}}_{W_t} \quad (\text{A.4})
 \end{aligned}$$

where  $\alpha \beta - \gamma^2$  is equal to  $A_t(\mathbf{s})$  in equation 3.5.

# Appendix B

## Synchronization Force Calculation

This appendix presents the manual synchronization force algorithm in commented pseudo code. The reader should also use the section 4.3.2 and especially figure 4.9 in parallel.

The variable *DecStart* is set to true when the decrease is started and the value  $F_{turn}$  is set as the actuator force request at the time of the start of the decrease. There is a counter outside this function which is enabled and reset by output signals.

```
% INPUTS
% F_reqOld - Last sample force request. If it is the first sample of
% the synchronization interval, this input is the requested force
% from the transportation PID controller of the last sample
% S - State of the state machine.
% w_i - Input shaft angular velocity
% w_o - Output shaft angular velocity
% RotSpeedReference - Reference value of the
% input shaft ang. velocity
% FirstSample - This input is one if it is the first
% sample of the synch. interval
% Counter - Value of the counter which is enabled
% by ClockEnable and Clock Reset

% OUTPUTS
% F_req - Requested force
% CounterEnable - Enables the counter which counts the number
% of samples the force request has been f_max
% CounterReset - Resets the same counter
```

If it is the first sample, the counter is reset and *DecStart* is set to false.

```

if FirstSample
    DecStart = false;
    CounterReset = true;
else
    CounterReset = false;
end

```

There are different maximum actuator force for the positive and negative side

```

if (S > 0)
    f_max = f_maxPos;
else
    f_max = f_maxNeg;
end

```

Slip and signum of slip calculation

```
slip = w_i - RotSpeedReference;
```

```

if (slip > 0)
    sgn_ws = 1;
else
    sgn_ws = -1;
end

```

The first step is to calculate area  $A_-$ . A local variable  $tempT$  is used to store the rest of the time of which the area  $A_-$  should be calculated.  $A_-$  is set to zero at the beginning.

```

tempT = T_d;
A_- = 0;
T_clock = Counter*T_sample;

```

The first test is if actual force request is in the interval between  $f_{end}$  and  $f_{ss}$  and "on its way down". A local variable  $Ftemp$  is used which is set to a value dependent on the turning value  $F_{turn}$ .

```

if (F_reqOld < f_ss && DecStart)

    Ftemp = min(F_turn, f_ss);

    % Check if the decrease of the force from Ftemp to
    % FreqOld takes longer or than T_d
    if (tempT < (Ftemp - F_reqOld)/k_sLo)
        A_- = tempT*(tempT*k_sLo/2 + F_reqOld);
        tempT = 0;
    else
        A_- = (Ftemp^2 - F_reqOld^2)/(2*k_sLo);
        tempT = tempT - (Ftemp - F_reqOld)/k_sLo;
    end
end

```

If the test was true,  $tempT$  is zero and the searched area is calculated and stored in  $A_-$ . Therefore, the following tests are always negative if  $tempT = 0$ .

Check the interval between  $f_{ss}$  and  $f_{max}$ .

```
if ((F_turn > f_ss)&&(F_reqOld < f_max)&&(tempT > 0)&&DecStart)
```

```
    Ftemp = min(F_turn, f_max);
```

```
    if (tempT < (Ftemp - max(F_reqOld, f_ss))/k_sHi)
```

```
        A_- = A_- + tempT*(tempT*k_sHi/2 + max(F_reqOld, f_ss));
```

```
        tempT = 0;
```

```
    else
```

```
        A_- = A_- + (Ftemp^2 - max(F_reqOld, f_ss)^2)/(2*k_sHi);
```

```
        tempT = tempT - (Ftemp - max(F_reqOld, f_ss))/k_sHi;
```

```
    end
```

```
end
```

Check if the last sample force request was  $f_{max}$  or if the decrease has started and  $tempT > 0$ .

```
if ((tempT > 0) && ((F_TurningValue == f_max ...
&& DecStart) || F_reqOld == f_max) )
```

```
    % check if the force has been f_max longer or
```

```
    % equal to the time of tempT
```

```
    if (T_clock >= tempT)
```

```
        A_- = A_- + f_max*tempT;
```

```
        tempT = 0;
```

```
    else
```

```
        A_- = A_- + f_max*T_clock;
```

```
        tempT = tempT - T_clock;
```

```
    end
```

```
end
```

Check if decrease has started and  $tempT$  is still larger than zero, or if last sample force request was larger than  $f_{ss}$  and  $tempT$  is greater than zero.

```
if ((tempT > 0)&&((F_turn >= f_ss && DecStart) || F_reqOld > f_ss))
```

```
    if (DecStart)
```

```
        Ftemp = min(F_TurningValue, f_max);
```

```
    else
```

```
        Ftemp = F_reqOld;
```

```
    end
```

```

if (tempT < (Ftemp - f_ss)/k_sHi)
  A_- = A_- + tempT*(Ftemp - k_sHi*tempT/2);
  tempT = 0;
else
  A_- = A_- + (Ftemp^2 - f_ss^2)/(2*k_sHi);
  tempT = tempT - (Ftemp - f_ss)/k_sHi;
end

```

end

The last interval to check is the one between the first sample force request, which is assumed to be  $f_0$ , and  $f_{ss}$ . If  $tempT$  is still larger than zero and decrease has started or if last sample force request is less than  $f_{ss}$ , another part should be added to  $A_-$ .

```

if (tempT > 0)

  if (DecStart)
    Ftemp = min(F_turn, f_ss);
  else
    Ftemp = min(F_reqOld, f_ss);
  end

  if (tempT < (Ftemp - f_0)/k_sLo)
    A_- = A_- + tempT*(Ftemp - k_sLo*tempT/2);
  else
    A_- = A_- + (Ftemp^2 - f_0^2)/(2*k_sLo);
  end
end

```

end

Here, the integrated requested actuator force, from  $T_d$  seconds backwards until present, is calculated as  $A_-$ .

Next step is to calculate the integrated force  $A_+$  from present until the force has reached the value  $f_{end}$ .

```

if (F_reqOld > f_ss)
  A_+ = (F_reqOld^2 - f_ss^2)/(2*k_sHi) ...
  + (f_ss^2 - f_end^2)/(2*k_sLo);
else
  A_+ = (F_reqOld^2 - f_end^2)/(2*k_sLo);
end

```

Calculate the total integrated force, the searched prediction of the input shaft angular velocity and  $A_s$  which is the integrated force from during the low slope value in figure 4.9 (i.e. if the synchronization force is  $f_{ss}$  at time  $T_{ss}$ , then  $A_s = \int_{T_{ss}}^{t+T_{end}} F_{s,s}(t)dt$ ).

---

```
ForceArea = A_a + A_b;
```

```
Constant = sgn_ws*r_m*my_cone/(J_input*sin(theta_cone));
```

```
OmegaSearched = w_i - Constant*ForceArea;
```

```
As = (f_ss^2 - f_end^2)/(2*k_sLo);
```

Left is to check if *OmegaSearched* has reached the searched value, and to calculate the force request.

```
if ((OmegaSearched <= RotSpeedReference + Omega_end && slip > 0) ...
|| (OmegaSearched >= RotSpeedReference - Omega_end && slip < 0) )
```

```
    % Decrease has started
```

```
    DecStart = true;
```

```
    Area_desired = abs((RotSpeedReference ...
+ sgn_ws*Omega_end - w_i)/(-Constant));
```

```
    if ( (Area_desired - A_-) >= As)
```

```
        F_req = min(sqrt( abs((Area_desired - A_- - As)* ...
... 2*k_sHi + f_ss^2) ), F_reqOld);
```

```
    else
```

```
        F_req = min(max( sqrt( abs((Area_desired - A_-)* ...
... 2*k_sLo + f_end^2) ), f_end), F_reqOld);
```

```
    end
```

```
elseif (DecStart)
```

```
    F_req = F_reqOld;
```

```
else
```

```
    % Ramp up the force request
```

```
    if (F_reqOld >= f_ss)
```

```
        F_req = min(T_sample*k_sHi + F_reqOld, f_max);
```

```
    else
```

```
        F_req = T_sample*k_sLo + F_reqOld;
```

```
    end
```

```
end
```

Finally, the counter is enabled if the force request has reached its maximum value  $f_{max}$ .

```
if (F_req >= f_max)
```

```
    CounterEnable = true;
```

```
else  
  CounterEnable = false;  
end
```

## Appendix C

# State Machine Functionality

This appendix includes a flowchart of the state transitions in the state machine and one table of functions used in it.

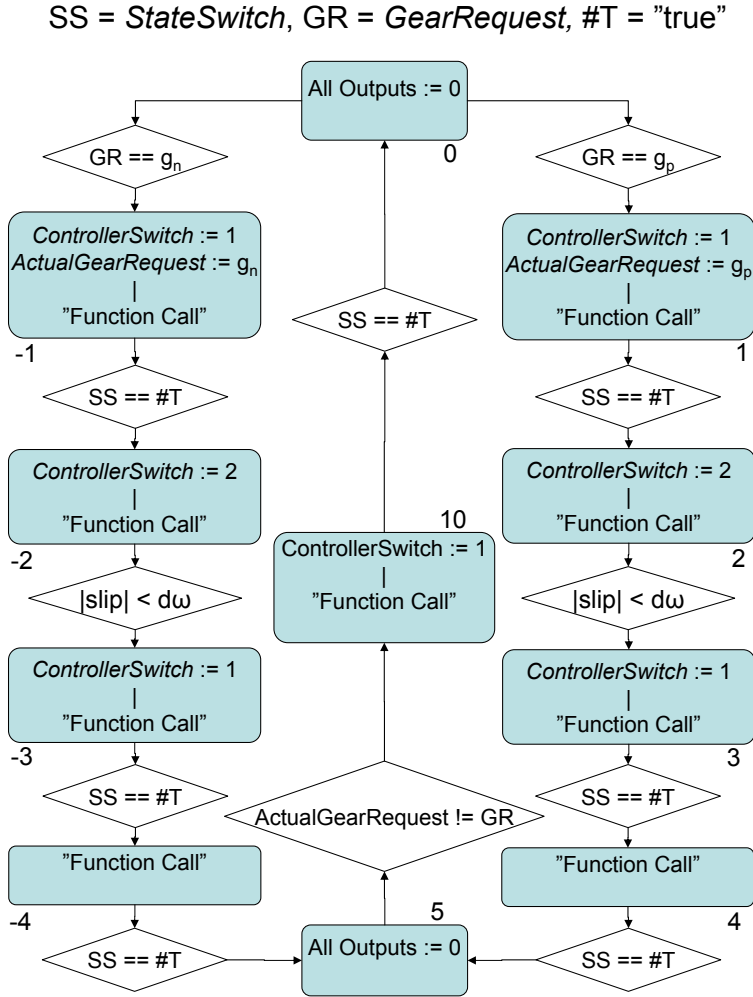


**Figure C.1.** A flowchart of the state machine. The value of *State* is displayed in the lower right corner of every box. All states corresponds to a separate interval, either a position interval or a slip interval. *ActualGearRequest* is a local variable, which is used in the transition between state 5 and 10 and also in state 10 to determine whether the disengagement takes place on the positive or negative side. The state machine can also switch from any of the states  $\pm 1 - \pm 4$  to state 10 in case of that the *GearRequest* changes before the gear is engaged. "Function Call" includes execution of the functions in table C.1. This execution is performed in every sample, and not only in the entry of the states.

Function name	State	Functionality/Task
<i>CalcPositionReference()</i>	$\pm 1, \pm 3, \pm 4, 10$	It ramps the <i>PositionReference</i> to a wanted value for the actual <i>State</i> . The slope of the ramped signal can be chosen and if a step is wanted, then a large value of the slope should be chosen.
<i>CalcBackPressure()</i>	All	Requested idle pressure calculation. In state 0 and 5, a zero pressure is wanted. In synchronization interval, the back pressure are decreased to zero when requested force is large enough. This enables maximum synchronization force. The pressure used in other cases are set in the initialization scripts and should be set to a value that enables enough braking force without any saturation of the active pressure line.
<i>CalcControlParams()</i>	$\pm 1, \pm 3, \pm 4, 10,$ ( $\pm 2$ if PID con- troller used in synch. inter- val)	Sets the output signal <i>ControllerParams</i> with actual PID parameters. There is also a counter which is cleared and enabled in the entry of every state. <i>CalcControlParams</i> compares the value of the counter and a user specified value. If the counter has exceeded the value, the integration part of the control parameters is set. Otherwise it is set to zero. This can be used to prevent a static error and the specified value, which corresponds to a specific time, can be tuned individually for every state, and should be set to zero if the integration part is desired from the beginning. (PID control can also be used for the synchronization interval and this function can be used also in state $\pm 2$ .)
<i>HandleCounter()</i>	$\pm 1, \pm 3, \pm 4, 10$	Starts another counter when the fork position is within a user specified interval of the reference position. Then the variable <i>StateShift</i> is set to <i>true</i> when the counter reaches another user specified value. It is cleared if the fork position leaves this interval before the counter has reached the specified time. This prevents a controller shift before the fork position is stable within a interval of the requested position.

**Table C.1.** Table of functions in the state machine. The explained functionality is individual for every value of *State*.